Effects of Deep-sea Anoxic Events on Thrust Faulting in Subduction Zone: Insights from the Jurassic Accretionary Complex in the Chichibu and Mino Belts

January 2021

Wang DING

Effects of Deep-sea Anoxic Events on Thrust Faulting in Subduction Zone: Insights from the Jurassic Accretionary Complex in the Chichibu and Mino Belts

A Dissertation Submitted to

the Graduate School of Life and Environmental Sciences,

the University of Tsukuba

in Partial Fulfillment of the Requirements

for the Degree of Doctor of Philosophy in Science

(Doctoral Program in Earth Evolution Sciences)

Wang DING

Contents

ABSTRACT

Pelagic sedimentary rocks in accretionary complexes record environmental changes during the oceanic plate migration from mid-oceanic ridge to trench. Recent studies have demonstrated that plate boundary faulting at shallow depth is highly localized along the characteristic lithology in pelagic sediments. However, it remains unknown whether shear localization also occurs in deeper portions. To elucidate the relationship between the environmental changes and the thrust faulting processes in subduction zone, I examined the pelagic sedimentary rocks in the Jurassic accretionary complex of the Chichibu and Mino Belts, central Japan.

In Lake Hamana area of the Chichibu Belt, the pelagic sedimentary rocks in the Jurassic accretionary complex preserve the lithostratigraphy composed of Lopingian (Upper Permian) gray chert, black chert, black claystone with a high carbon content of 4.86–6.78 wt%, siliceous claystone, black chert, and Anisian (Middle Triassic) gray chert, in ascending order. The symmetric in the lithostratigraphy and the change in the radiolarian ages with respect to black carbonaceous claystone are presumed to represent the deep-sea anoxic event that occurred across the Permian–Triassic boundary. The black carbonaceous claystone suffered from an intense shear, resulting in blocks of siliceous claystone in the scaly black claystone matrix. The localization of shear along black carbonaceous claystone likely represents lower frictional strength of clay-rich rocks than surrounding quartz-rich siliceous rocks.

In Inuyama area of the Mino Belt, the coherent chert-clastic rocks are imbricated along the thrust faults branched from the plate-boundary fault. The stratigraphy at the lowermost part of the thrust sheet consists of, in ascending order, black carbonaceous claystone, siliceous claystone, black chert, and gray chert, representing the Early to Middle Triassic recovery from the deep-sea superanoxia. The detailed field mapping of the fault zone at the lowermost part of the thrust sheet indicates the localization of shear along black carbonaceous claystone layers, which is marked by intensely developed scaly fabric. The discrete slip surface developed within the black carbonaceous claystone. The Raman spectra of carbonaceous material demonstrate a slight increase of carbonization on the discrete slip surface relative to the surrounding scaly carbonaceous claystone, suggesting a temperature increase during localized slip.

These results indicate that the localization of thrust faulting also occurred in deeper portions of the subduction zone and is intimately linked to the black carbonaceous claystone accumulated during deep-sea anoxic events. The increased heating recorded on the discrete slip surface may be accommodated by a seismic slip in deeper portions of the subduction zone.

Key words: Deep-sea anoxic event; P-Tr boundary; black claystone; Lake Hamana; plate boundary faulting; fault zone structure; Raman Spectra

List of Figures

List of Tables

Chapter 1: Preservation of Permian-Triassic Boundary Section in the Jurassic Accretionary Complex of the Lake Hanama, Central Japan

1.1 Introduction

The largest mass extinction in Earth's history occurred across the Permian–Triassic (P–Tr) boundary, with up to 96% of all marine species and 70% of terrestrial vertebrate species becoming extinct (Benton, 2015; Sahney and Benton, 2008). Investigation of geological records at that time is undoubtedly the key to elucidate the causes of this catastrophe. The reconstructed Late Permian–Early Jurassic paleogeography is characterized by the presence of the superoceans Paleo-Tethys and Panthalassa. P-Tr boundary sequences in the Paleo-Tethys have been studied more extensively than those in the Panthalassa due to the better preservation of Paleo-Tethys sequences.

Previous studies on the shallow-sea facies successions around the Paleo-Tethyan regions suggested that biotic mass extinction was simultaneous with the extreme environments including; global warming as a consequence of Siberian Traps (Burgess et al., 2017; B. Chen et al., 2013; Z. Q. Chen et al., 2018; Grasby et al., 2017; Wang et al., 2018; Joachimski et al., 2012; Romano et al., 2013; Sun et al., 2012), ocean acidification (Clarkson et al., 2013), and poorly oxygenated water (Wignall and

Twitchett, 1996; Grice et al., 2005).

On the other hand, the deep-sea sedimentary rocks in the superocean Panthalassa are presumed to record a long term deep-sea anoxic event from Late Permian to Middle Triassic (Isozaki, 1994, 1997). A schematic deep-sea P–Tr boundary section consists of red chert, gray chert, siliceous claystone, carbonaceous claystone, siliceous claystone, gray chert, and red chert, in ascending order (Isozaki, 1997). The symmetrical change in lithology with respect to carbonaceous claystone is assumed to represent a deep-sea anoxic event which occurred across the P–Tr boundary in the superocean Panthalassa. However, the complete Panthalassan P–Tr section has been rarely preserved in the pelagic sedimentary rocks, primarily due to the development of plate-boundary décollements along the carbonaceous claystone, separating accreted Triassic pelagic sediments above subducting Permian sediments below (Nakae, 1993; Wakita, 2012). The schematic deep-sea P–Tr boundary section has therefore been largely constructed from a compilation of stratigraphic columns in different regions.

Pelagic sedimentary rocks accumulated in the superocean Panthalassa are distributed in the Jurassic accretionary complex in Japan (Isozaki et al., 1990). Based on paleontological, lithostratigraphic and geochemical evidences, sections including or neighboring the P-Tr boundary were recognized from the Jurassic accretionary complex in several areas (Muto et al., 2018 and references therein). In the Lake Hamana area of central Japan, Permian, Triassic, and Jurassic radiolarians can be found in chert and siliceous mudstone (Hori, 2008; Niwa and Tsukada, 2004; Ieda, 2001; Mizugaki, 1985).

In addition, “Toishi-type” siliceous claystone, which has been found near the P-Tr boundary, is distributed in the western (Suse Unit and Tame Unit in Hori, 2008) and eastern (Outcrop C in Ieda, 2001) sides of Lake Hamana. Therefore, the P–Tr boundary was expected to be preserved in the Lake Hamana area.

This chapter examined the lithostratigraphy, deformation structures, and radiolarian ages preserved in the pelagic sedimentary rocks of the Hamanako section. Lithostratigraphy and radiolarian ages of the section were subsequently correlated to other deep-sea P–Tr boundary sections within the Jurassic accretionary complex, Japan. As a result, I suggest that the complete pelagic P–Tr boundary section has been preserved in the Hamanako section despite suffering from complex mélange forming processes in the accretionary complex.

1.2 Geological setting

The Jurassic accretionary complex in Japan is mainly composed of Permian basalt-limestone-chert, Permian–Triassic siliceous claystone, Middle Triassic–Early Jurassic chert, Early-Middle Jurassic siliceous mudstone, and Jurassic to Early Cretaceous terrigenous sediments (Wakita, 2012). The chert and siliceous claystone originally accumulated in a pelagic open-ocean setting in the superocean Panthalassa, after which they traveled with the migration of the oceanic plate to trench and accreted onto the microcontinent in the Late Jurassic, forming part of the accretionary complex (Isozaki et al., 1990; Matsuda and Isozaki, 1991; Isozaki et al., 2010; Taira et al., 2016). The Jurassic accretionary complex in the Chichibu Belt of central Japan consists of the mélange, represented by tabular basalt, limestone, and chert blocks in an argillaceous matrix (Figure 1-1). The Jurassic accretionary complex has a fault contact with the Sambagawa metamorphic rocks (Figure 1-1b).

Northeast of the Lake Hamana area, the Jurassic accretionary complex is divided into two units: the Iinoya and Miyakoda Formations (Saito, 1955; Makimoto et al., 2004; Niwa, 2004; Niwa and Tsukada, 2004) (Figure 1-1b). The Iinoya Formation structurally overlies the Miyakoda Formation and is characterized by basalt, limestone, and chert blocks in a mudstone matrix. The chert and mudstone yield Middle Triassic and Middle Jurassic radiolarian fossils, respectively (Ieda and Sugiyama, 1998; Makimoto et al., 2004; Mizugaki, 1985). The Miyakoda Formation is marked by chert blocks and sandstone blocks in a mudstone matrix (Makimoto et al., 2004; Niwa, 2004).

Guadalupian–Lopingian (Middle-Upper Permian) to Middle-Upper Triassic radiolarians have been reported in Miyakoda cherts (Ieda, 2001; Mizugaki, 1985), while the Middle Jurassic radiolarian fossils have been reported in Miyakoda mudstones (Niwa and Tsukada, 2004).

The studied Hamanako section located along the northeast lakeshore of the Lake Hamana, 40 km northwest of Hamamatsu City in Shizuoka Prefecture, Tokai Region, Central Japan (Figure 1-1b). The section lies within a chert block of the Miyakoda Formation and is surrounded by Quaternary terrace deposits. This chert block yielded Permian, Triassic, and Jurassic radiolarians from several scattered localities (Ieda, 2001). Late Permian radiolarians were also reported in the southern part of the Hamanako section (Ieda, 2001).

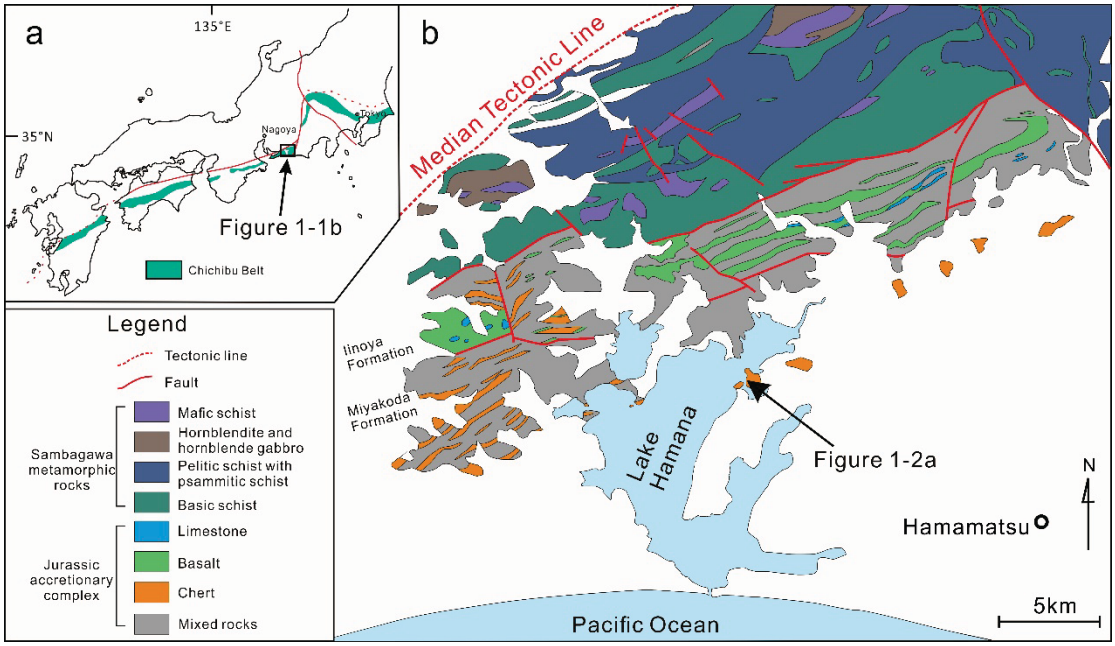

Figure 1-1 (a) Distribution of the Chichibu Belt in Japan (modified from Isozaki et al., 2010). (b) Geological map of the Jurassic accretionary complex and Sambagawa metamorphic rocks near the Lake Hamana (modified from Makimoto et al., 2004; Niwa and Tsukada, 2004). Note that the size of sandstone blocks in mixed rocks is too small to show in Figure 1-1b.

1.3 Lithostratigraphy and deformation structures

The pelagic sedimentary rocks in the Hamanako section moderate to steeply dipping to the north-northwest, consistent with the general trend of the Jurassic accretionary complex in the Chichibu Belt, central Japan (Figures 1-1b, 1-2a). From south to north, the lithology changes from gray chert to black chert, terrigenous rocks composed of sandstone and mudstone, black claystone, siliceous claystone, black chert, terrigenous rocks consisting of sandstone and mudstone, and gray chert (Figure 1-2). Small faults are also present in the section. Figures 1-2b, 1-3, and 1-4 show the column sections, representative outcrops, and microstructural features of each lithology, respectively.

Bedded gray chert is distributed across the southern part of the section (Figures 1-2b, 1-3a). Under the microscope, gray chert is composed of microcrystalline quartz, thin quartz veins, and radiolarian tests (Figure 1-4a). Ieda (2001) reported lower Lopingian radiolarians from the gray chert (Figure 1-2). The gray chert is overlain by bedded black chert (Figure 1-3b). The black chert contains radiolarian tests and carbonaceous materials which have been cut or displaced by the quartz veins (Figure 1-4b).

A 1 m thick unit of terrigenous rocks can be seen above the gray chert exhibiting shear deformation characterized by sandstone clasts in a mudstone matrix (Figures 1-3c, 1-4c, and 1-5a). Slickenlines and slickensteps are visible on the polished surface (Figure 1-6a). The sandstone clasts have an asymmetric shape defined by a right-lateral

shear sense (Figures 1-5a, 1-5c, 1-6b).

Sheared black claystone and gray siliceous claystone overlie the terrigenous rocks and are characterized by blocks of siliceous gray claystone in a black claystone matrix (Figure 1-5a). The black claystone matrix is intensely sheared along an anastomosing scaly foliation (Figure 1-3d), displaying a composite-planar fabric defined by P-foliation and Y-shear (Figures 1-4d, 1-6c). The shear sense, determined from the slickenlines and the asymmetric fabrics, indicates right-lateral shear (Figures 1-4d, 1-5b, 1-6c). The black claystone primarily consists of quartz, illite, pyrite, and carbonaceous material. The carbon contents of four black claystone samples (Figure 1-5a), measured by a Yanaco CHN corder MT-6 elemental analyzer, range between 4.85–6.78 wt% (Table 1-1).

The sheared black claystone and the gray siliceous claystone are overlain by relatively coherent siliceous claystone (Figure 1-3e). The siliceous claystone is greenish to grayish in color and is mainly composed of quartz, clay mineral, and pyrite. Radiolarian tests are rare in the siliceous claystone. The anastomosing dark seams are locally developed in the siliceous claystone (Figure 1-4e). The color and mineral composition of the siliceous claystone are similar to those of the “Toishi-type” siliceous claystone distributed near the P–Tr boundary (Imoto, 1984; Musashino, 1993; Motoki and Sashida, 2004; Suzuki et al., 1998).

A second bedded black chert unit (Figure 1-3f) overlies the siliceous claystone; the chert contains microcrystalline quartz, radiolarian tests, and carbonaceous materials

(Figure 1-4f). The 2 m thick siliceous claystone is intercalated in the bedded black chert.

Terrigenous rocks were recognized above the bedded black chert (Figure 1-3g). The rocks contain fine- to medium-grained, well-sorted sand grains that are mixed with mud (Figure 1-4g).

Bedded gray chert is distributed in the uppermost part of the section (Figure 1-3h) and is comprised of microcrystalline quartz and radiolarian tests (Figure 1-4h). Asymmetric folds have developed in gray chert (Figure 1-2).

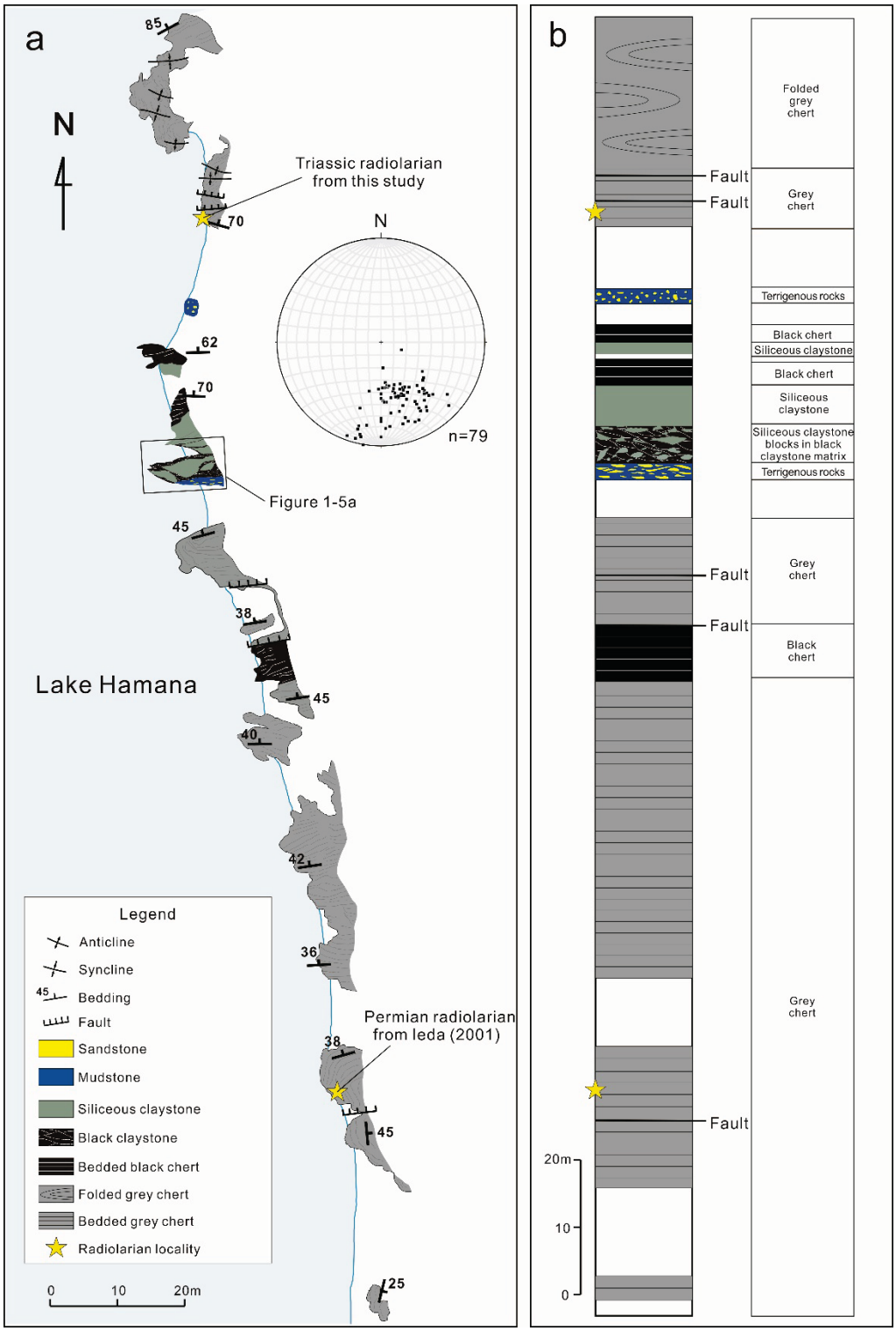

Figure 1-2 (a) Route map of the Hamanako section (inset: lower hemisphere equal-area stereoplots showing the orientations of the bedding); the location of the map is shown in Figure 1-1b. (b) Column section showing the lithostratigraphy in the Hamanako section; yellow stars indicate the horizons where Permian and Middle Triassic radiolarians were reported from Ieda (2001) and this study, respectively.

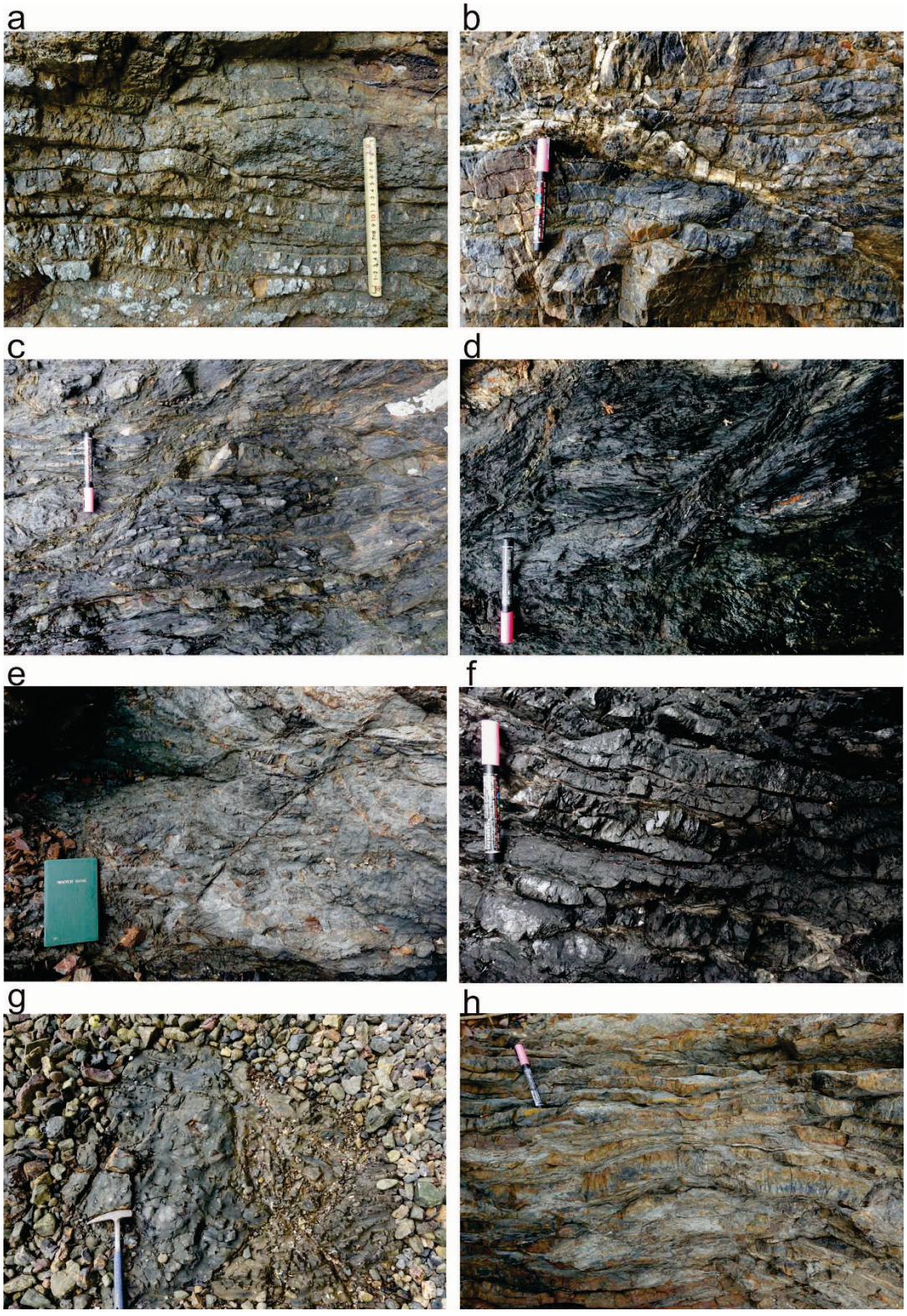

Figure 1-3 Representative lithology in the Hamanako section. (a) Lower bedded gray chert. (b) Lower bedded black chert. (c) Sheared terrigenous rocks. (d) Scaly black claystone. (e) Siliceous claystone. (f) Upper bedded black chert. (g) Terrigenous rocks composed of sandstone and mudstone. (h) Upper bedded gray chert.

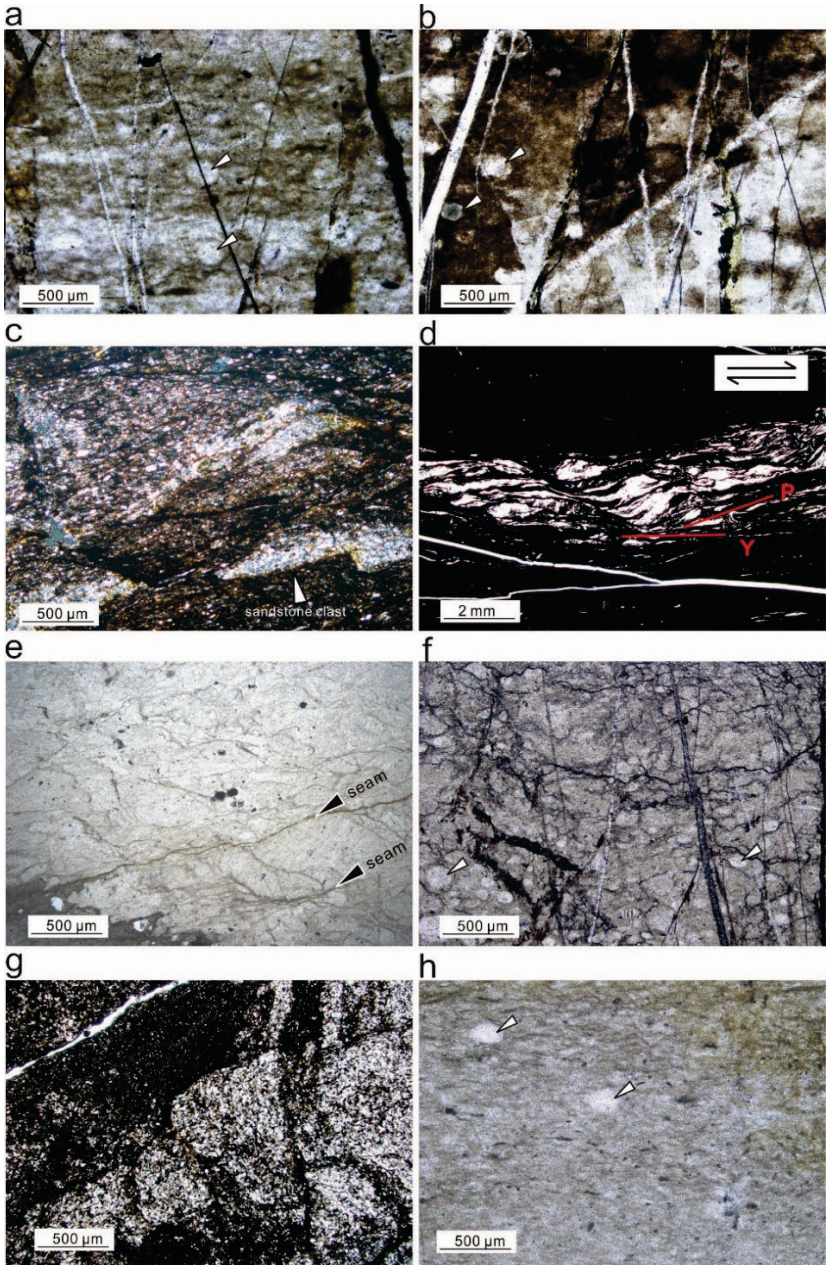

Figure 1-4 Photomicrographs of representative lithology in the Hamanako section. White triangles in Figures 1-4a, 1-4b, 1-4f, and 1-4h indicate radiolarian tests. (a) Gray chert mainly composed of microcrystalline quartz and radiolarian tests. (b) Black chert showing opaque carbonaceous materials and radiolarian tests cut by quartz veins. (c) Terrigenous rocks showing sandstone clasts in the mudstone matrix. (d) Black claystone. Fragmented quartz veins in the dark matrix showing a P-Y fabric. Half arrows indicate sense of shear. (e) Siliceous claystone in which anastomosing dark seams are recognized. (f) Black chert composed of microcrystalline quartz and abundant radiolarian tests. (g) Clastic rocks including sand grains in mud. (h) Gray chert composed of microcrystalline quartz and radiolarian tests.

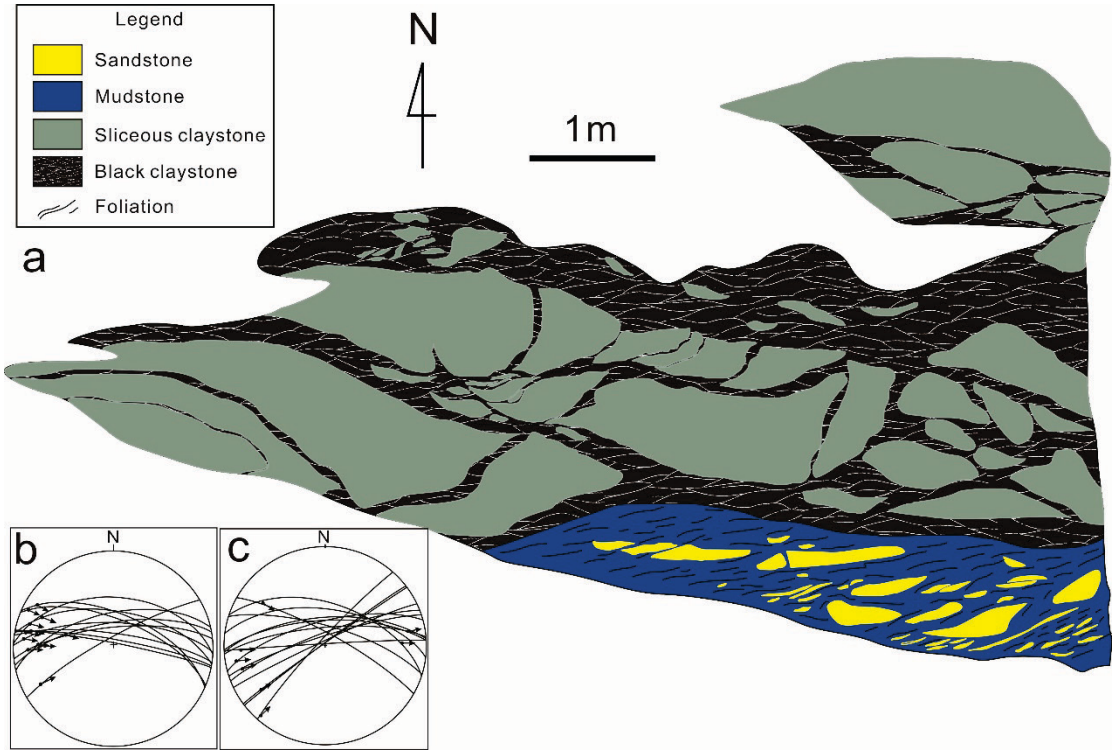

Figure 1-5 (a) Occurrence of shear zones characterized by siliceous claystone blocks in a black claystone matrix and sandstone blocks in a mudstone matrix. The location is shown in Figure 1-2a. Lower hemisphere equal-area projection of shear surfaces (girdles) and slickenline (dots) in black claystone (b) and mudstone (c). Arrows indicate shear direction.

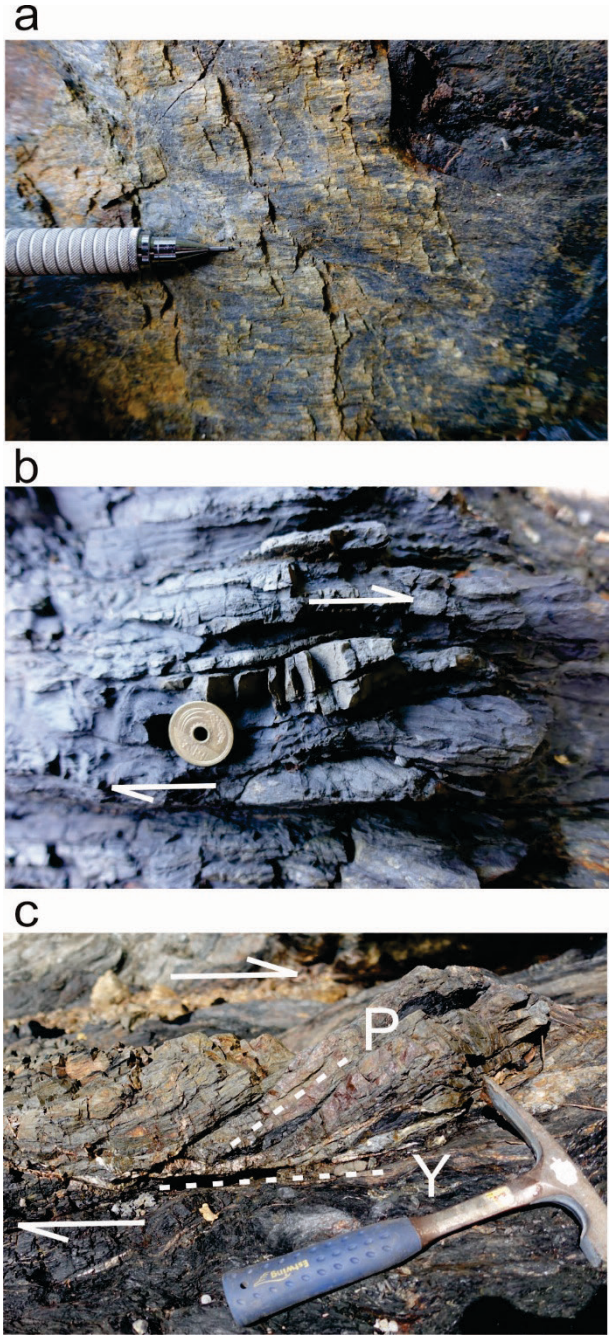

Figure 1-6 Deformation in shear zones. Half arrows indicate the sense of shear. (a) Slickenlines and steps developed on mudstone. (b) Asymmetric sandstone clasts in a mudstone matrix. (c) Siliceous claystone blocks in a black claystone matrix, showing a P-Y fabric.

Table 1-1 Total organic carbon (TOC) content of black claystone from the Hamanako section

Sample	TOC (wt%)
TC1-1	6.78
TC1-2	6.43
TC2-1	4.85
TC2-2	4.90

1.4 Radiolarian biostratigraphy and faunal age

Ieda (2001) reported radiolarians *Albaillella sp*. cf. A. *triangularis* Ishiga, Kito, and Imoto from the gray cherts in the lower part of the section (Figure 1-2). In southwest Japan, the radiolarian *Neoalbaillella optima* Assemblage Zone is characterized by *Albaillella triangularis* (Kuwahara et al., 1998; Kuwahara and Yamakita, 2001), indicating an age of lower Lopingian (Kuwahara et al., 1998; Sano et al., 2012).

The identification of specific level from the newly obtained radiolarian tests was difficult for the black chert, black claystone, and siliceous claystone due to poor preservation. However, the gray chert in the upper part of the section (Figure 1-2) yielded abundant radiolarians: *Plafkerium? antiquum* Sugiyama, *Nofrema? gigantoceras* Sugiyama, *Tiborella argia* Sugiyama, *Hozmadia gifuensis* Sugiyama, *Archaeosemantis* sp., and *Tetrarhopalus?* sp. (Figure 1-7). The occurrence range of these species coincides with that of the TR2A (the *Eptingium nakasekai* group lowest-occurrence zone) to TR3A (the Spine A2 lowest-occurrence zone) (Sugiyama, 1997). The first appearance of *Hozmadia gifuensis* Sugiyama, characteristic species of the TR2A, indicates an age of early Anisian (Sugiyama, 1992, 1997).

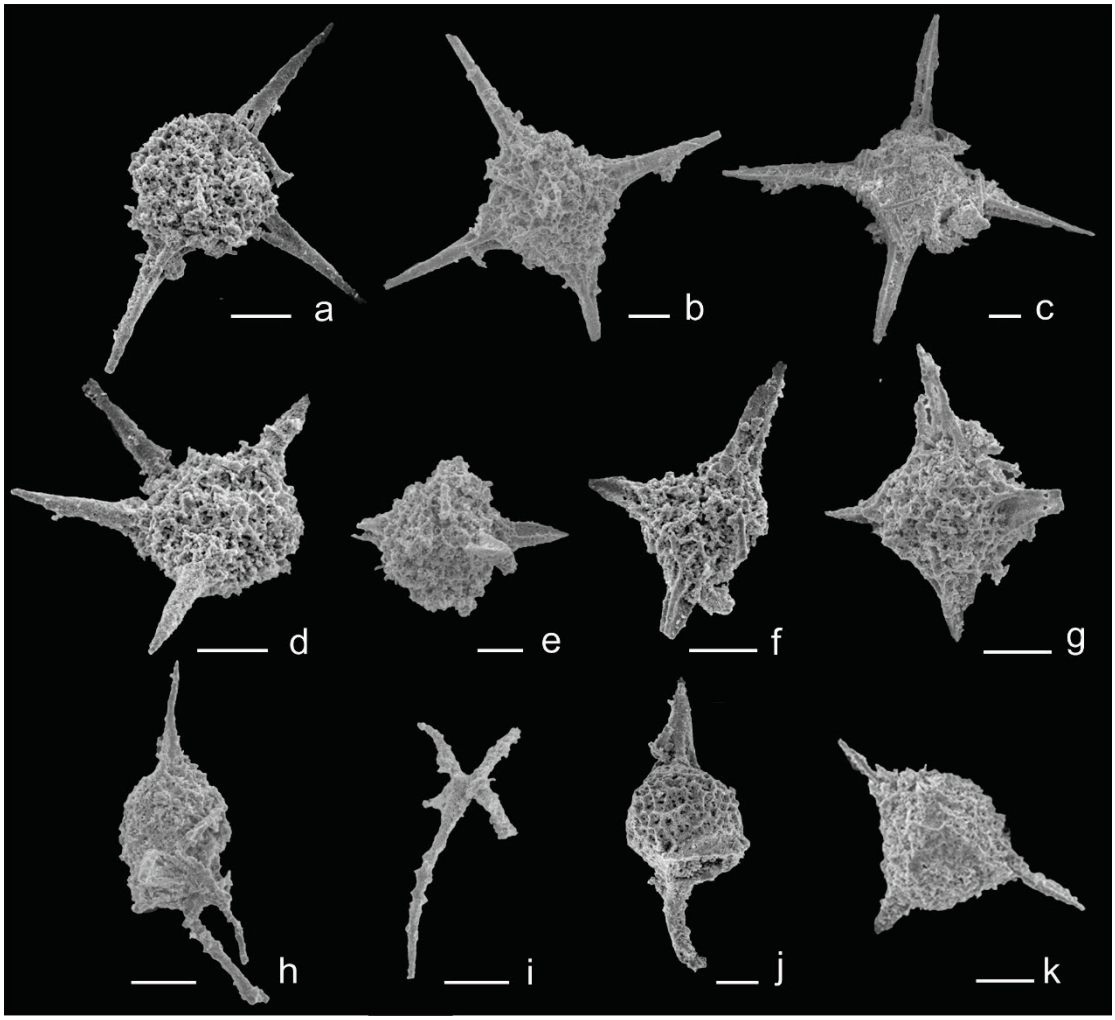

Figure 1-7 SEM microphotographs of Triassic radiolarian fossils obtained from gray chert in the upper part of the Hamanako section. White scale bars, 50 μm. (a–d) *Plafkerium? antiquum* Sugiyama; (e–g) *Tiborella argia* Sugiyama; (h) *Nofrema? gigantoceras* Sugiyama; (i) *Archaeosemantis* sp.; (j) *Hozmadia gifuensis* Sugiyama; (k) Tetrarhopalus? sp..

1.5 Discussion

1.5.1 Stratigraphic correlations and the deep-sea facies P–Tr boundary

The lithostratigraphy preserved in the pelagic sedimentary rocks in the Hamanako section is consistent with the schematic deep-sea P–Tr boundary section, which records gray chert, black chert, siliceous claystone, black chert, and gray chert, in ascending order (Isozaki, 1997). The presence of the Lopingian radiolarians in the lower gray chert (Ieda, 2001) and the Anisian radiolarians in the upper gray chert (Figure 1-2b) in the Hamanako section suggests that the P–Tr boundary is placed in the black claystone. Although the exact age of the newly obtained radiolarians and conodonts was hard to determine, the stratigraphic horizon of the "Toishi-type" siliceous claystone was correlated to the Lower Triassic due to its position below the Anisian radiolarian-bearing gray chert (Figure 1-2b).

The deep-sea anoxic event lasted approximately 20 Myr from the Lopingian to Anisian (Kato et al., 2002; Suzuki et al., 1998), during which chert deposition was replaced by siliceous claystone deposition (Isozaki, 1997). The anoxic event across the P–Tr boundary intensified at the end of the Permian into a deep-sea setting (Isozaki, 1997). The elevated marine primary productivity associated with the blooming of anaerobic plankton and bacteria in that time led to the production of abundant carbonaceous materials, which resulted in the deposition of black carbonaceous claystone (Ishiga, 1994; Isozaki, 1997). Thus, the high carbon content (4.85–6.78 wt%) in the black claystone likely represents the climax of the anoxic event near the P–Tr

boundary.

The deposition timing of the black carbonaceous claystone may be constrained from other sections in the Jurassic complex. In the Ubara and Tenjinmaru sections, the transition from siliceous claystone to black carbonaceous claystone could be correlated to the upper Permian, and a reverse change to the Lower Triassic (Kakuwa, 2008). In the Akkamori section, concentration of redox-sensitive trace elements also indicates that the anoxic condition recorded in the black carbonaceous claystone ranges from Changhsingian (Upper Permian) to Griesbachian (Lower Triassic) (Takahashi et al., 2009). Therefore, based on stratigraphic correlation, the black carbonaceous claystone likely preserves the P-Tr boundary.

In addition, increased carbon content is another good indicator that the P-Tr boundary has been preserved in the black carbonaceous claystone, having also been reported from other P–Tr boundary intervals preserved in the Jurassic accretionary complex of Japan (Suzuki et al., 1998; Takahashi et al., 2009; Yamakita et al., 1999). For example, carbon contents in Tenjinmaru and Akkamori sections were 1.2–2.5 wt% and 1.0–2.0 wt%, respectively, compared to less than 1.0 wt% in the surrounding siliceous claystone (Suzuki et al., 1998; Takahashi et al., 2009). The carbon contents in the Hamanako section are higher than in the Tennjinmaru and Akkamori sections, which reflect the spatial variations or fluctuation of oxygenation levels of deep-sea conditions during the deposition of the black carbonaceous claystone in the Panthalassa.

The lithostratigraphy identified from the Hamanako section is correlated to other

deep-sea P–Tr boundary sections in the Jurassic accretionary complex (Figure 1-8). In the Ubara, Funabuseyama, and Akkamori sections, the first appearance datum of conodont *Hindeodus parvus* (Kozur and Pjatakova) suggests that P–Tr boundary is placed in black claystone between the Lopingian siliceous claystone and Lower Triassic siliceous claystone (Sano et al., 2010; Takahashi et al., 2009; Yamakita et al., 1999). Although *H. parvus* has not been recognized in the Tenjinmaru and Nakaoi sections, the siliceous claystone directly below the black claystone yields conodonts of possible Lopingian age (Kuwahara and Yamakita, 2001). Only the Triassic rocks exposed in the Konose and Shakuma 2 sections, and siliceous claystone has not been recognized in the Shakuma 1 and Hikodake sections. Thus, in addition to the Funabuseyama section, the Hamanako section likely records almost the entire sequence from the Lopingian to Anisian rocks. The integration of lithostratigraphy, radiolarian ages, and high carbon content of black claystone therefore suggests a potential deep-sea facies P–Tr boundary in the Hamanako section.

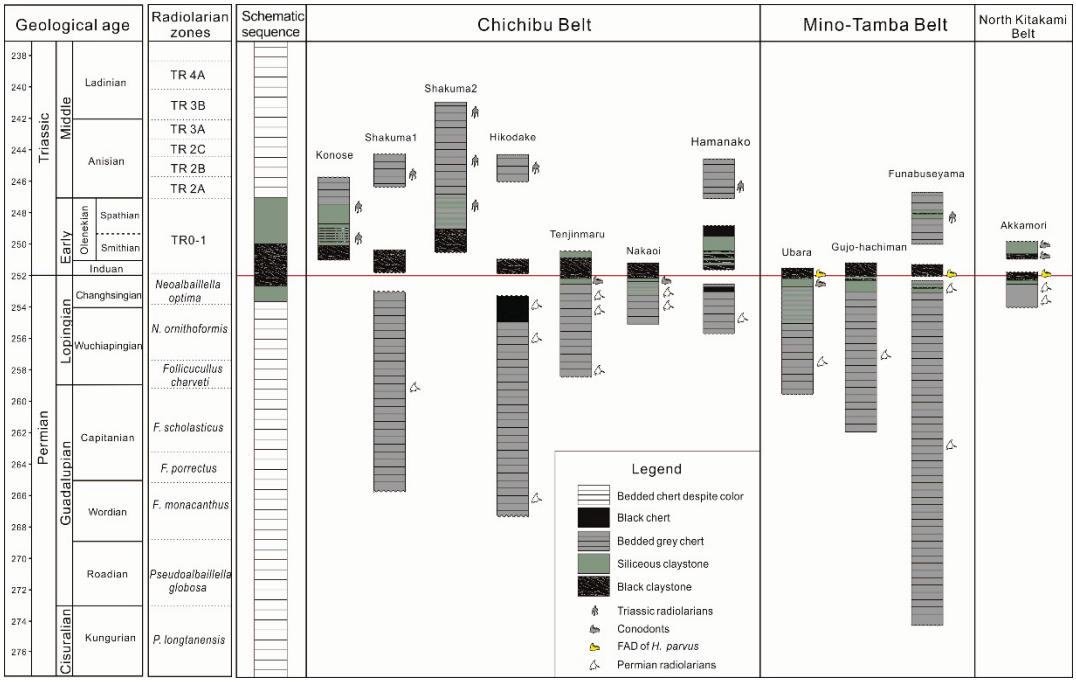

Figure 1-8 Correlations of the P–Tr boundary sections in Japan. The time scale is based on International Chronostratigraphic Chart v 2020/01 (Cohen et al., 2013, updated January 2020). Radiolarian zones are after Ishiga (1986), Ito and Matsuoka (2018), Kuwahara et al., (1998), Sugiyama (1997), and Zhang et al., (2014). Schematic sequence is after Isozaki (1997). The Konose, Shakuma, and Hikodake sections are after Nishizono et al., (1996); the Tenjinmaru section after Kuwahara and Yamakita (2001), Yamakita (1987); the Nakaoi section after Kuwahara and Yamakita (2001); the Ubara section after Kuwahara et al., (1991), Kuwahara and Yamakita (2001), Tada et al., (2005), and Yamakita et al., (1999); the Gujo-hachiman section after Algeo et al., (2010), Kuwahara et al., (1991, 1998), Kuwahara and Yamakita (2001), and Tada et al., (2005); the Funabuseyama section after Kuwahara et al., (2010), Sano et al., (2010); the Akkamori section after Ehiro et al., (2008), Takahashi et al., (2009, 2010); and the Hamanako section is based on this study.

1.5.2. Preservation of deep-sea P–Tr boundary section

In the Hamanako section, the shear is highly localized along the black claystone, resulting in incorporation of siliceous claystone blocks in the black claystone matrix. This shear localization may be due to the high clay content in the black claystone relative to the surrounding quartz-rich siliceous rocks, because the frictional strength decreases with an increase in clay content (Tembe et al., 2010).

The plate-boundary décollement tends to be localized along a weak layer, such as a smectite-rich pelagic clay (Chester et al., 2013; Kameda et al., 2015; Ujiie et al., 2013; Vrolijk, 1990). In the case of the Jurassic accretionary complex in central Japan, the décollement has been considered to have been localized along the P–Tr boundary claystone (Nakae, 1993; Wakita, 2012). Shear localization along the black claystone is consistent with the décollement localization along the P–Tr boundary. Because the sediments above the décollement are scraped off or underplated into an overlying accretionary prism, the entire deep-sea P–Tr boundary section is rarely preserved.

While the Hamanako section may preserve the deep-sea P–Tr boundary section, it also includes terrigenous rocks showing sandstone blocks in a mudstone matrix. The Jurassic accretionary complex in the Chichibu Belt, central Japan is characterized by a mélange composed of sandstone, mudstone, chert, limestone, and basalt (Niwa, 2004) (Figure 1-1b). The blocks of chert in the mélange are laterally continuous, in which the original stratigraphy is well preserved. Although the chert in the Lake Hamana area is surrounded by Quaternary terrace deposits, the local occurrence of terrigenous rocks in

the Hamanako section may represent the mixing of terrigenous rocks into the chert block that preserves the P–Tr boundary section. The mélanges in the Jurassic accretionary complexes are interpreted as the result of complex, multiple deformation processes including submarine sliding, mud diapirism, shearing along the décollement, and out-of-sequence thrust (Wakita, 2012). The chert block may behave as a relatively strong competent block, and thus survived from intense deformation during the mélange-forming processes, resulting in preservation of the P–Tr boundary section.

1.6 Conclusion

A new P–Tr boundary section was found from the chert block of the Jurassic accretionary complex of Lake Hamana area. The P–Tr boundary section is characterized by symmetry in the lithostratigraphy and a change in radiolarian ages with respect to black claystone with high carbon content, which represent a deep-sea anoxic event that occurred across the P–Tr boundary. The shear is highly localized along the P–Tr boundary black carbonaceous claystone, possibly owing to a high clay content relative to the surrounding siliceous rocks. The intercalated terrigenous rocks may represent the mixing of terrigenous and pelagic rocks during the mélange forming processes.

References

Algeo, T. J., Hinnov, L., Moser, J., Maynard, J. B., Elswick, E., Kuwahara, K. and Sano, H. (2010). Changes in productivity and redox conditions in the Panthalassic Ocean during the latest Permian. Geology, 38(2), 187–190.

Benton, M. J. (2015). When Life Nearly Died: The Greatest Mass Extinction of All Time. Thames & Hudson.

Burgess, S. D., Muirhead, J. D. and Bowring, S. A. (2017). Initial pulse of Siberian Traps sills as the trigger of the end-Permian mass extinction. Nature Communications, 8(1), 1–4.

Chen, B., Joachimski, M. M., Shen, S. Z., Lambert, L. L., Lai, X. L., Wang, X. D., Chen, J. and Yuan, D. X. (2013). Permian ice volume and palaeoclimate history: Oxygen isotope proxies revisited. Gondwana Research, 24(1), 77–89.

Chen, Z.Q., Zhao, L., Wang, X., Luo, M. and Guo, Z. (2018). Great Paleozoic-Mesozoic biotic turnings and paleontological education in China: A tribute to the achievements of Professor Zunyi Yang. Journal of Earth Science, 29(4), 721–732.

Chester, F. M., Rowe, C., Ujiie, K., Kirkpatrick, J., Regalla, C., Remitti, F., Moore, J. C., Toy, V., Wolfson-Schwehr, M., Bose, S., Kameda, J., Mori, J. J., Brodsky, E. E., Eguchi, N., Toczko, S. and Expedition 343 & 343TScientists. (2013). Structure and Composition of the Plate-Boundary Slip Zone for the 2011 Tohoku-Oki Earthquake. Science, 342(6163), 1208–1211.

Clarkson, M. O., Richoz, S., Wood, R. A., Maurer, F., Krystyn, L., McGurty, D. J. and Astratti, D. (2013). A new high-resolution $\delta^{13}C$ record for the Early Triassic: insights from the Arabian Platform. Gondwana Research, 24(1), 233-242.

Cohen, K. M., Finney, S. C., Gibbard, P. L., & Fan, J. X. (2013; updated January 2020). The ICS International Chronostratigraphic Chart. Episodes 36, 199–204.

Ehiro, M., Yamakita, S., Takahashi, S., & Suzuki, N. (2008). Jurassic accretionary complexes of the North Kitakami Belt in the Akka-Kuji area, Northeast Japan. The Journal of the Geological Society of Japan, 114, 121–139.

Grasby, S. E., Shen, W., Yin, R., Gleason, J. D., Blum, J. D., Lepak, R. F., Hurley, J. P. and Beauchamp, B. (2017). Isotopic signatures of mercury contamination in latest Permian oceans. Geology, 45(1), 55–58.

Grice, K., Cao, C., Love, G. D., Böttcher, M. E., Twitchett, R. J., Grosjean, E., Summons, R. E., Turgeon, S. C., Dunning, W., and Jin, Y. (2005). Photic zone euxinia during the Permian-Triassic superanoxic event. Science, 307(5710), 706-709.

Hori, R. (2008) Geology of the Toyohashi and Tahara districts, Chapter 3. Quadrangle Series, 1: 50,000, Geological Survey of Japan, AIST, 1-6.

Ieda, K. (2001). Radiolarians from the Chichibu terrane in western part of Hamamatsu City, Shizuoka Prefecture, Japan. Science Report of the Toyohashi Museum of Natural History, 11, 23–26.

Ieda, K. and Sugiyama, K. (1998). Triassic radiolarians from the Chichibu terrane in eastern Toyohashi City. Science Report of the Toyohashi Museum of Natural History,

8, 17–21.

Imoto, N. (1984). Late Paleozoic and Mesozoic cherts in the Tamba Belt, Southwest Japan (Part 1). Bulletin of Kyoto University of Education. Series B, 65, 15–40.

Ishiga, H. (1986). Late Carboniferous and Permian Radiolarian Biostratigraphy of Southwest Japan. Journal of Geosciences, Osaka City University, 29, 89–100.

Ishiga, H. (1994). Permian/Triassic boundary and carbon circulation in pelagic sediments of Southwest Japan. Earth Science (Chikyu Kagaku), 48(4), 285–297.

Isozaki, Y., Maruyama, S. and Furuoka, F. (1990). Accreted oceanic materials in Japan. Tectonophysics, 181(1–4), 179–205.

Isozaki, Y. (1994). Superanoxia across the Permo-Triassic boundary: record in accreted deep-sea pelagic chert in Japan.

Isozaki, Y. (1997). Permo-Triassic boundary superanoxia and stratified superocean: Records from lost deep sea. Science, 276(5310), 235–238.

Isozaki, Y., Aoki, K., Nakama, T. and Yanai, S. (2010). New insight into a subduction-related orogen: A reappraisal of the geotectonic framework and evolution of the Japanese Islands. Gondwana Research, 18(1), 82–105.

Ito, T. and Matsuoka, A. (2018). Lithology and radiolarian age of the Ryokami-yama Chert Formation in eastern Mt. Ryokami: Possible décollement zone in Permian pelagic sequence in mid-Mesozoic accretionary complexes of Southwest Japan. Island Arc, 27(6), 1–15.

Joachimski, M. M., Lai, X., Shen, S., Jiang, H., Luo, G., Chen, B., Chen, J. and Sun, Y.

(2012). Climate warming in the latest Permian and the Permian-Triassic mass extinction. Geology, 40(3), 195–198.

Kakuwa, Y. (2008). Evaluation of palaeo-oxygenation of the ocean bottom across the Permian–Triassic boundary. Global and Planetary Change, 63(1), 40-56.

Kameda, J., Shimizu, M., Ujiie, K., Hirose, T., Ikari, M., Mori, J., Oohashi, K. and Kimura, G. (2015). Pelagic smectite as an important factor in tsunamigenic slip along the Japan Trench. Geology, 43(2), 155–158.

Kato, Y., Nakao, K. and Isozaki, Y. (2002). Geochemistry of Late Permian to Early Triassic pelagic cherts from southwest Japan: implications for an oceanic redox change. Chemical Geology, 182(1), 15–34.

Kuwahara, K., Nakae, S. and Yao, A. (1991). Late Permian “Toishi-type” siliceous mudstone in the Mino-Tamba Belt. The Journal of the Geological Society of Japan, 97(12), 1005–1008.

Kuwahara, K., Sano, H., Ezaki, Y. and Yao, A. (2010). Discovery of Triassic siliceous rocks within a large Permian oceanic-rock mass in the Mt. Funabuseyama area, western Mino terrane, and geologic implication. The Journal of the Geological Society of Japan, 116(3), 159–173.

Kuwahara, K. and Yamakita, S. (2001). Microbiostratigraphy on chert facies of Upper Permian in the Northern Chichibu Belt, Shikoku, Southwest Japan. News of Osaka Micropaleontologists, Special Volume, 12, 51–59.

Kuwahara, K., Yao, A. and Yamakita, S. (1998). Reexamination of Upper Permian

radiolarian biostratigraphy. Earth Science (Chikyu Kagaku), 52(5), 391–404.

Makimoto, H., Yamada, N., Mizuno, K., Takada, A., Komazawa, M. and Sudo, S. (2004). Geological Map of Japan 1:200,000, Toyohashi and Irago Misaki. Geological Survey of Japan, AIST.

Matsuda, T. and Isozaki, Y. (1991). Well-documented travel history of Mesozoic pelagic chert in Japan: From remote ocean to subduction zone. Tectonics, 10(2), 475–499.

Mizugaki, K. (1985). Radiolarian fossils from the Chichibu system, northwest of Hamana Lake, central Japan. Bulletin of the Mizunami Fossil Museum, 12, 171–182.

Motoki, H. and Sashida, K. (2004). Preliminary report on the chronological and lithostratigraphical studies of the Toishi-type shale (siliceous claystone) distributed in the Ashio Mountains, central Japan. News of Osaka Microplaeontologists, Special Volume, 13, 47–57.

Musashino, M. (1993). Chemical composition of the “Toishi-type” siliceous shale. Part 1. Bulletin of the Geological Survey of Japan, 44(12), 699–705.

Muto, S., Takahashi, S., Yamakita, S., Suzuki, N., Suzuki, N. and Aita, Y. (2018). High sediment input and possible oceanic anoxia in the pelagic Panthalassa during the latest Olenekian and early Anisian: Insights from a new deep-sea section in Ogama, Tochigi, Japan. Palaeogeography, palaeoclimatology, palaeoecology, 490, 687-707.

Nakae, S. (1993). The Permo-Triassic boundary as a decollement zone within pelagic siliceous sediments, with reference to Jurassic accretion of the Tamba Terrane, SW Japan. Bulletin of the Geological Survey of Japan, 44(7), 471–481.

Nishizono, Y., Yoshida, H. and Murata, M. (1996). The siliceous rock facies near the Permo-Triassic (P/T) boundary in the Southern Chichibu Terrane, Kyushu. The Journal of the Geological Society of Japan, 102(7), 591–608.

Niwa, K. (2004). Re-division of the Chichibu belt of the western area of Lake Hamana, central Japan. Bulletin of the Nagoya University Museum, 20, 71–78.

Niwa, K. and Tsukada, K. (2004). Jurassic radiolarian fossils from the Miyakoda Formation in the Lake Hamana area, Shizuoka Prefecture, central Japan. The Journal of Earth and Planetary Sciences, Nagoya University, 51, 1–10.

Romano, C., Goudemand, N., Vennemann, T. W., Ware, D., Schneebeli-Hermann, E., Hochuli, P. A., Brühwiler, T., Brinkmann, W. and Bucher, H. (2013). Climatic and biotic upheavals following the end-Permian mass extinction. Nature Geoscience, 6(1), 57–60.

Sahney, S. and Benton, M. J. (2008). Recovery from the most profound mass extinction of all time. Proceedings of the Royal Society B: Biological Sciences, 275(1636), 759-765.

Saito, M. (1955). Geology of the Mikawa-ono district. With Geological Sheet Map at 1:50,000. Geological Survey of Japan, AIST.

Sano, H., Kuwahara, K., Yao, A. and Agematsu, S. (2010). Panthalassan seamount-associated Permian-Triassic boundary siliceous rocks, Mino terrane, central Japan. Paleontological Research, 14(4), 293–314.

Sano, H., Kuwahara, K., Yao, A. and Agematsu, S. (2012). Stratigraphy and age of the

Permian-Triassic boundary siliceous rocks of the Mino terrane in the Mt. Funabuseyama area, central Japan. Paleontological Research, 16(2), 124-145.

Sugiyama, K. (1992). Lower and Middle Triassic Radiolarians from Mt. Kinkazan, Gifu Prefecture, Central Japan. In Transactions and proceedings of the Paleontological Society of Japan. 1992(167), 1180-1223.

Sugiyama, K. (1997). Triassic and Lower Jurassic radiolarian biostratigraphy in the siliceous claystone and bedded chert units of the southeastern Mino Terrane, Central Japan. Bulletin of the Mizunami Fossil Museum, 24, 79–193.

Sun, Y., Joachimski, M. M., Wignall, P. B., Yan, C., Chen, Y., Jiang, H. and Lai, X. (2012). Lethally hot temperatures during the Early Triassic greenhouse. Science, 338(6105), 366–370.

Suzuki, N., Ishida, K., Shinomiya, Y. and Ishiga, H. (1998). High productivity in the earliest Triassic ocean: Black shales, Southwest Japan. Palaeogeography, Palaeoclimatology, Palaeoecology, 141(1–2), 53–65.

Tada, R., Watanabe, S., Kashiyama, Y., Tajika, E., Kato, T., Yamamoto, S., Isozaki, Y., & Sakuma, H. (2005). High-resolution analysis of Late Paleozoic-Early Mesozoic variability of paleoceanographic system recorded in bedded chert sequence in the inner zone of Southwest Japan. Journal of Geography, 114(4), 638–642.

Taira, A., Ohara, Y., Wallis, S. R., Ishiwatari, A. and Iryu, Y. (2016). Geological evolution of Japan: an overview. The Geology of Japan; Moreno, T., Wallis, SR, Kojima, T., Gibbons, W., Eds, 1-24.

Takahashi, S., Kaiho, K., Oba, M. and Kakegawa, T. (2010). A smooth negative shift of organic carbon isotope ratios at an end-Permian mass extinction horizon in central pelagic Panthalassa. Palaeogeography, Palaeoclimatology, Palaeoecology, 292(3–4), 532–539.

Takahashi, S., Yamakita, S., Suzuki, N., Kaiho, K. and Ehiro, M. (2009). High organic carbon content and a decrease in radiolarians at the end of the Permian in a newly discovered continuous pelagic section: A coincidence? Palaeogeography, Palaeoclimatology, Palaeoecology, 271(1–2), 1–12.

Tembe, S., Lockner, D. A., & Wong, T. F. (2010). Effect of clay content and mineralogy on frictional sliding behavior of simulated gouges: Binary and ternary mixtures of quartz, illite, and montmorillonite. Journal of Geophysical Research: Solid Earth, 115(3), 1–22.

Ujiie, K., Tanaka, H., Saito, T., Tsutsumi, A., Mori, J. J., Kameda, J., Brodsky, E. E., Chester, F. M., Eguchi, N., Toczko, S. and Expedition 343 & 343T Scientists. (2013). Low coseismic shear stress on the Tohoku-Oki megathrust determined from laboratory experiments. Science, 342(6163), 1211–1214.

Vrolijk, P. (1990). On the mechanical role of smectite in subduction zones. Geology, 18(8), 703–707.

Wakita, K. (2012). Mappable features of mélanges derived from Ocean Plate Stratigraphy in the Jurassic accretionary complexes of Mino and Chichibu terranes in Southwest Japan. Tectonophysics, 568–569, 74–85.

Wang, X., Cawood, P. A., Zhao, H., Zhao, L., Grasby, S. E., Chen, Z. Q., Wignall, P. B., Lv, Z., and Han, C. (2018). Mercury anomalies across the end Permian mass extinction in South China from shallow and deep water depositional environments. Earth and Planetary Science Letters, 496, 159–167.

Wignall, P. B. and Twitchett, R. J. (1996). Oceanic anoxia and the end Permian mass extinction. Science, 272(5265), 1155-1158.

Yamakita, S. (1987). Stratigraphic relationship between Permian and Triassic strata of chert facies in the Chichibu Terrane in eastern Shikoku. The Journal of the Geological Society of Japan, 93, 145–148.

Yamakita, S., Kadota, N., Kato, T., Tada, R., Ogihara, S., Tajika, E. and Hamada, Y. (1999). Confirmation of the Permian/Triassic boundary in deep-sea sedimentary rocks; earliest Triassic conodonts from black carbonaceous claystone of the Ubara section in the Tamba Belt, Southwest Japan. The Journal of the Geological Society of Japan, 105(12), 895–898.

Zhang, L., Ito, T., Feng, Q. L., Caridroit, M. and Danelian, T. (2014). Phylogenetic model of Follicucullus lineages (Albaillellaria, Radiolaria) based on high-resolution biostratigraphy of the Permian Bancheng Formation, Guangxi, South China. Journal of Micropalaeontology, 33(2), 179–192.

Chapter 2: Plate Boundary Processes in the Deeper Portion of the Cold Subduction Zone: An Example from the Fault Zone in the Jurassic Chert-clastic Complex, Central Japan

2.1 Introduction

Deep ocean drilling has demonstrated that the plate-boundary faulting at shallow depths in the Japan Trench subduction zone is highly localized along the smectite-rich pelagic clay, where a huge coseismic slip occurred during the 2011 Tohoku-Oki earthquake (Chester et al., 2013; Ujiie et al., 2013). Localization of the plate-boundary faulting was also confirmed in the northern Barbados subduction zone, which is marked by the development of scaly foliated radiolarian claystone constituting a low bulk density zone relative to surrounding sediments (Labaume et al., 1997; Moore et al., 1998; Moore and Klaus, 2000). While deep ocean drilling in subduction zones contributed to a better understanding of the plate-boundary faulting processes in shallow portions, those in deeper portions have not been examined well.

Exhumed accretionary complexes allow the examination of the plate-boundary processes in deeper portions of subduction zones, including coseismic deformation. Pseudotachylyte (i.e., solidified frictional melt) is the most reliable geological evidence for seismic slip (Cowan, 1999; Rowe and Griffith, 2015). Although the pseudotachylytes have also been found in exhumed accretionary complexes (Ujiie and Kimura, 2014 and references therein), they are rarely preserved in recognizable forms

due to hydrothermal alteration and devitrification in subduction zones (Ishikawa and Ujiie, 2019). Recent fault rock studies and the friction experiments on fault zone materials demonstrated that the Raman spectra of carbonaceous material (RSCM) are useful in detecting the increased heating on faults (Furuichi et al., 2015; Ito et al., 2017; Kuo et al., 2014, 2017; Oohashi et al., 2011; Ujiie et al., 2021). The fault zone in the Jurassic chert-clastic complex, central Japan includes carbonaceous mudstone. The Jurassic chert-clastic complex is considered to represent the on-land analog of deeper portions of the cold subduction zone such as the Japan Trench (Yamaguchi et al., 2016).

This chapter presents the deformation and kinematics recorded in the fault zone, and provide the RSCM of the fault rocks. Based on the results, we discuss the plate-boundary processes in deeper portions of the cold subduction zone.

2.2 Geological setting

The coherent chert-clastic complex exposed along the Kiso River in the Inuyama area preserves the ocean plate stratigraphy, which comprises, in ascending order, Early to Middle Triassic siliceous claystone, Middle Triassic to Early Jurassic pelagic chert, Middle Jurassic siliceous mudstone, and Middle-early Late Jurassic sandstone and mudstone (Figure 2-1) (Kimura & Hori, 1993; Matsuda and Isozaki, 1991; Yao, 1980). This ocean plate stratigraphy was repeated by thrust faults (Figure 2-1c). Matsuda and Isozaki (1991) interpreted that the thrusts were formed in associated with duplex underplating, whereas Kimura and Hori (1993) considered that the thrust faults are out-of-sequence thrusts bounding pelagic sedimentary rocks above from clastic rocks below. Pelagic sedimentary rocks have a characteristic lithology composed of, in ascending order, siliceous claystone including carbonaceous mudstone, black chert, gray chert, and red chert, which are considered to represent the recovery from the deep-sea anoxic events (Isozaki, 1997). The maximum attained temperature of the chert-clastic complex, determined from the chlorite geothermometer and vitrinite reflectance, is approximately 220 °C (Kameda et al., 2012).

The studied fault zone was developed along the thrust fault, which bounds the pelagic sedimentary rocks in the thrust sheet 3 above from clastic rocks in the thrust sheet 2 below (Figures 2-1c, 2-2). The clastic rocks in sheet 2 are Middle to early Late Jurassic in age (Yao, 1980), whereas the pelagic sedimentary rocks in sheet 3 are mainly composed of the late Early Triassic (Spathian) to the early Middle Triassic (Anisian)

gray and black chert, and the middle-late Early Triassic (Smithian to Spathian) siliceous claystone (Takahashi et al., 2010, 2015; Yamakita et al., 2010, 2016).

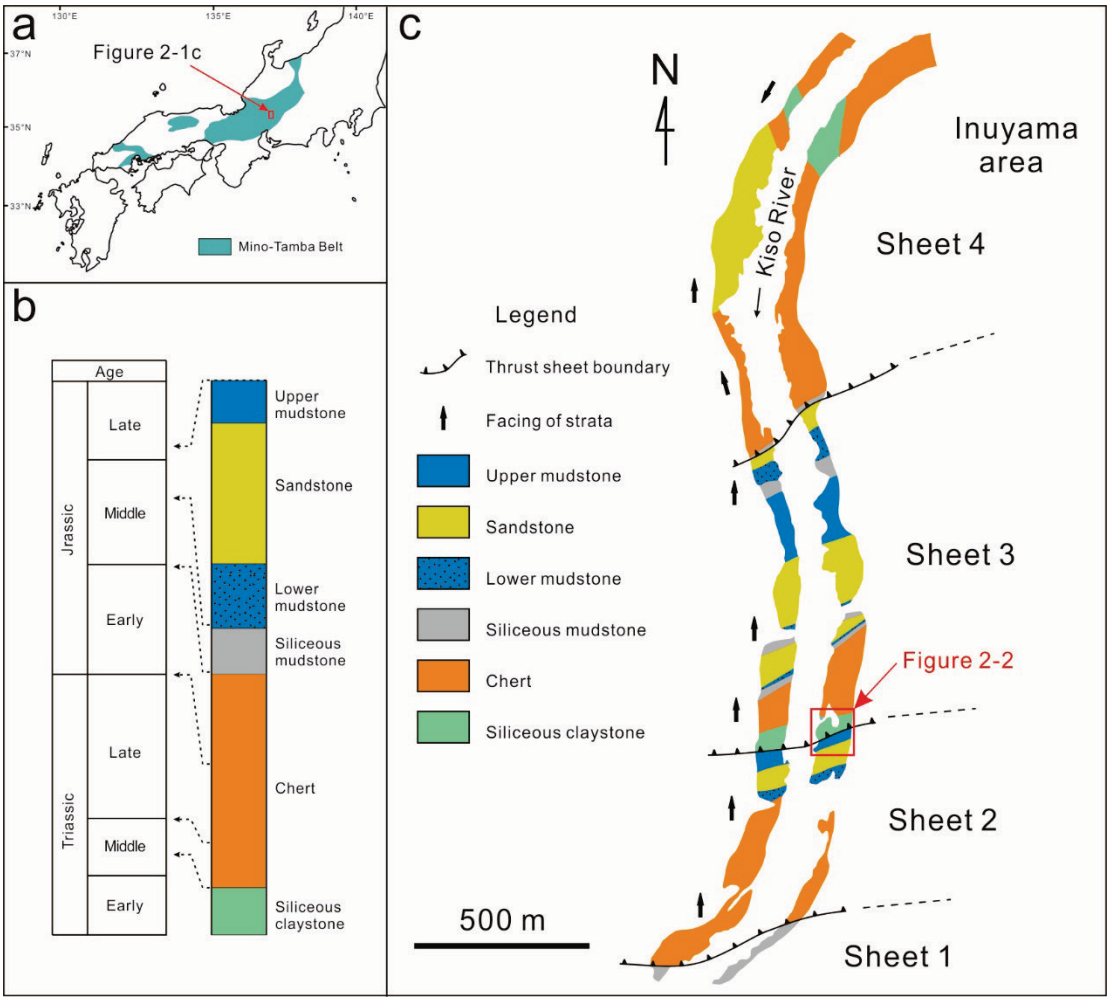

Figure 2-1 (a) Distribution of the Mino-Tamba Belt in Japan. (b) Reconstructed ocean plate stratigraphy in the Inuyama area, modified from Kimura and Hori (1993). (c) Geological map of the chert-clastic sequence along the Kiso River in the Inuyama area, modified from Kimura and Hori (1993). The location of the figure is shown in Figure 2-1a.

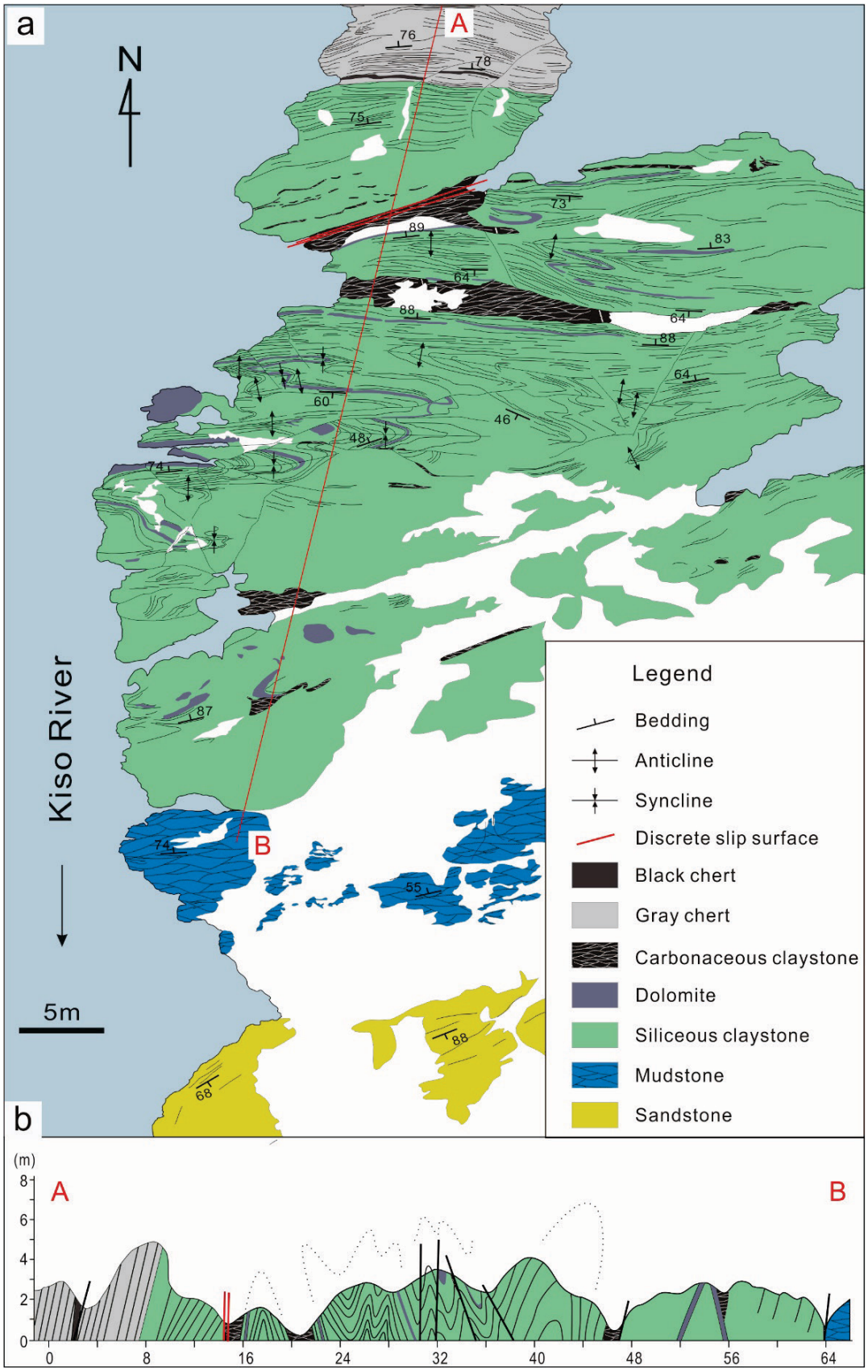

Figure 2-2 (a) Geological map (a) and cross section (b) of the fault zone. The location of the geological map is shown in Figure 2-1c.

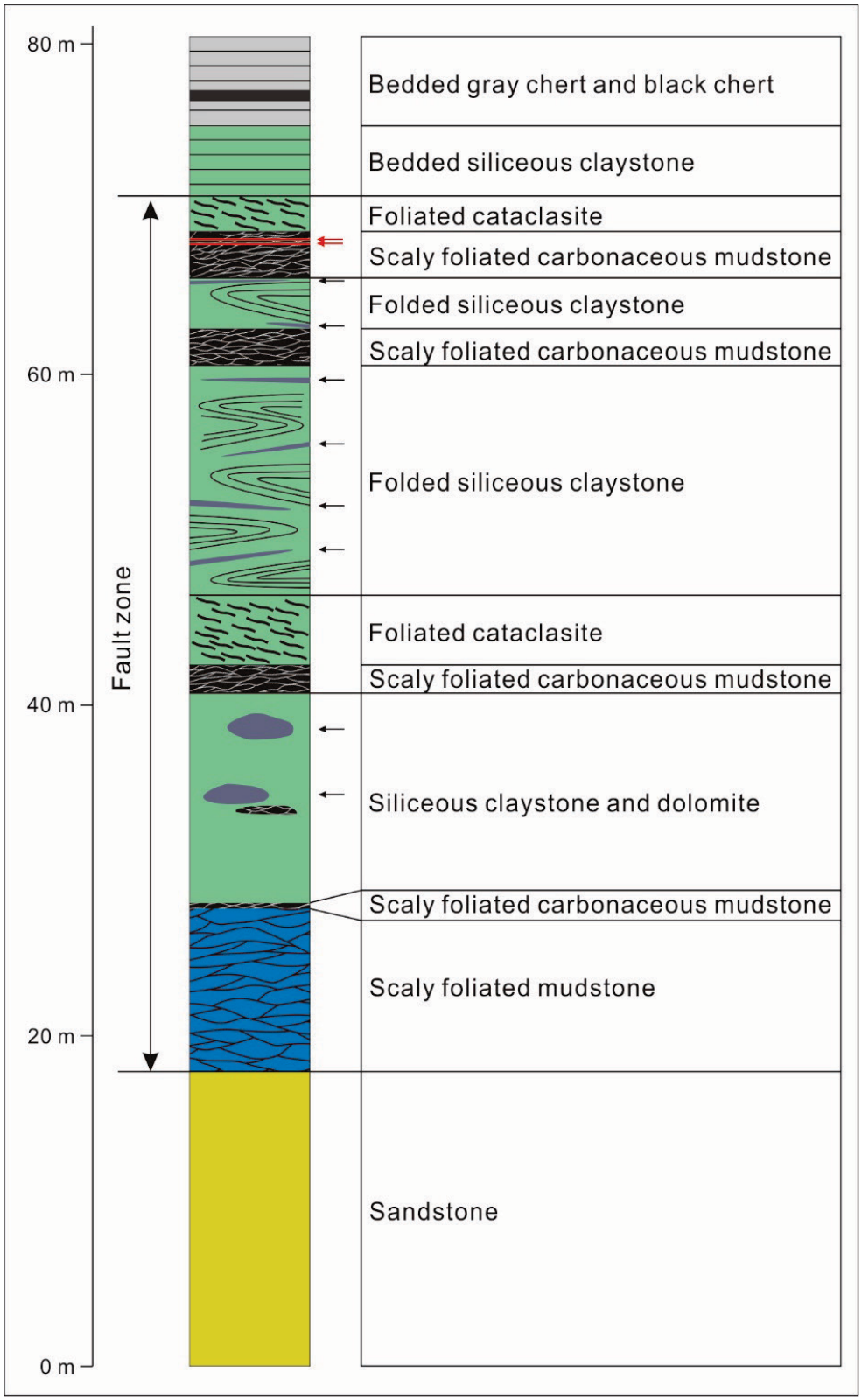

Figure 2-3 Column section of the fault zone. Black arrows indicate dolomite intercalated in siliceous claystone. Red arrows indicate the discrete slip surfaces.

2.3 Deformation structures and kinematic in the fault zone

The ~50 m thick fault zone is defined by the development of scaly fabrics in the upper mudstone and black carbonaceous claystone, and foliated cataclasite derived from siliceous claystone and black carbonaceous claystone (Figures 2-2, 2-3). Folded siliceous claystone and dolomite are intercalated in the fault zone. The fault zone is flanked by sandstone in sheet 2 and bedded siliceous claystone, gray and black chert in sheet 3.

The scaly fabric in the upper mudstone shows ~1–2 cm spaced anastomosing foliation (Figure 2-4a). Slickenlines and steps were recognized on the polished surfaces (Figure 2-4b).

Black carbonaceous claystone is distributed at four horizons in the fault zone (Figures 2-2, 2-3), representing the zones of shear concentration. However, it is also locally scattered in siliceous claystone (Figure 2-2). The deformation in the black carbonaceous claystone is also marked by the development of the scaly fabric. The scaly fabric shows ~1–5 mm spaced anastomosing foliation (Figure 2-4c) or the composite planar fabric. The scaly foliation is polished and lineated (Figure 2-4d). The slip directions determined from slickenlines on the foliation and composite plane fabric show both reverse slip and left-lateral slip (Figure 2-4g).

Two discrete slip surfaces sharply cut the scaly foliated black carbonaceous claystone, representing a localization of slip with respect to the surrounding distributed shear along the scaly fabric (Figure 2-4e). The discrete slip surfaces are polished, and

slickenlines on the surfaces indicate left-lateral slip (Figures 2-4h, 2-5a). Energy dispersive X-ray spectrometry mapping indicates the relative enrichment of Al and K along the discrete slip surface, suggesting the relative concentration of illite (Figure 2-5b).

The foliated cataclasite is defined by the alignment of fragmented siliceous claystone and black carbonaceous claystone (Figure 2-4f) and is distributed above the scaly foliated black carbonaceous claystone. The thickness of the foliated cataclasite ranges 1–4 m.

The folds in the siliceous claystone are close to tight (Figure 2-6a). The axial surfaces of folds are vertical, and the fold axes strike east-west and shallowly plunge toward WSW or ESE (Figure 2-6b). The orientations of the fold axes and the asymmetric fold geometry indicate top-to-the-south shear. The ~10–15 cm-thick dolomite layers are also folded with siliceous claystone (Figure 2-2).

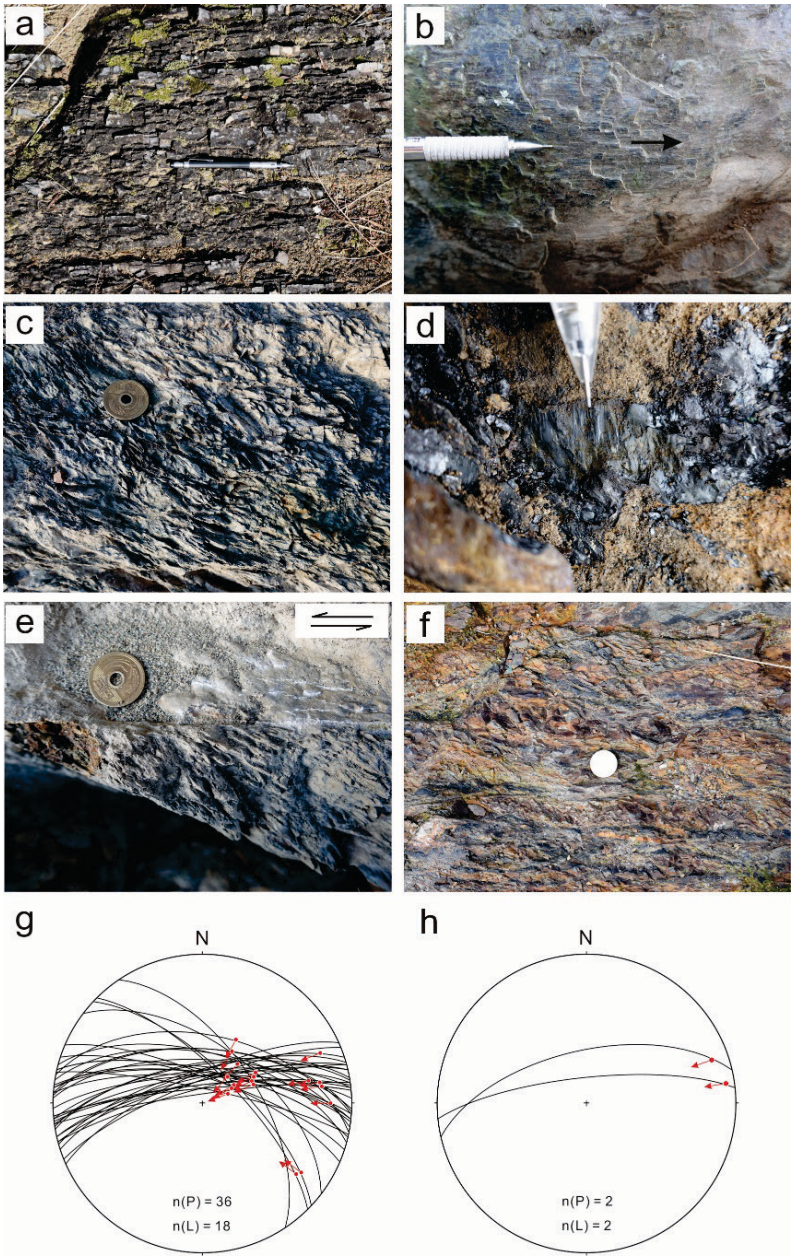

Figure 2-4 (a) Scaly fabric in upper mudstone. (b) Scaly foliation surface in upper mudstone showing slickenlines and steps. (c) Scaly carbonaceous claystone exhibiting anastomosing foliation. (d) Slickensides within scaly carbonaceous claystone. (e) Discrete slip surface sharply cutting the scaly carbonaceous claystone. The half-arrows indicate the sense of shear. (f) Foliated cataclasite showing a mixture of siliceous claystone and black carbonaceous claystone. (g) Slip directions of scaly upper mudstone and scaly foliated carbonaceous claystone; lower hemisphere, equal-area projection. Red arrows indicate the movement direction of the hanging wall. (h) Slip directions for discrete slip surfaces; lower hemisphere, equal-area projection. Red arrows indicate the movement direction of the hanging wall.

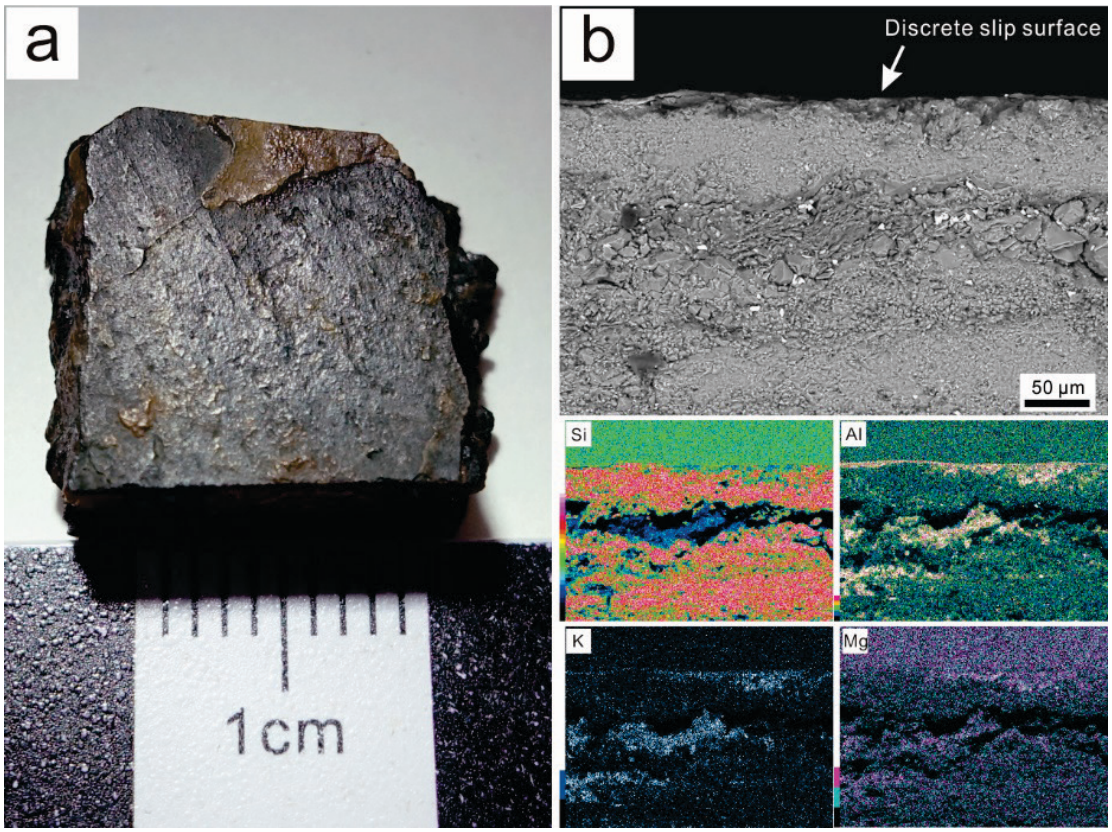

Figure 2-5 (a) Occurrence of discrete slip surface showing polished and lineated surface. (b) Back-scattered electron image and the EDS elemental map of the discrete slip surface and underlying scaly carbonaceous claystone.

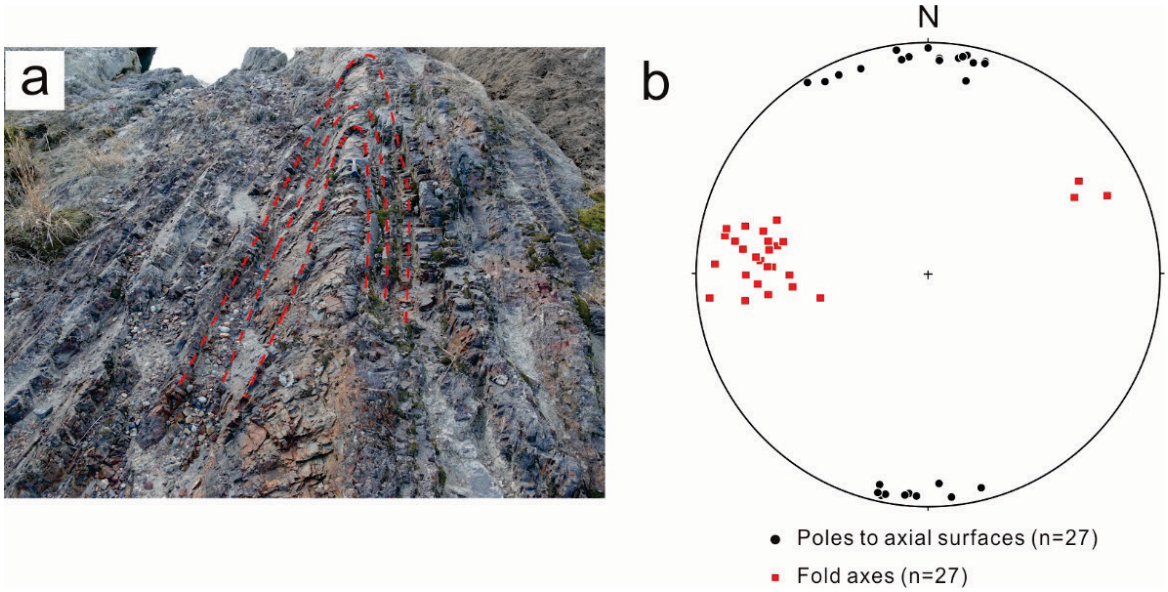

Figure 2-6 (a) Occurrence of folds in siliceous claystone. (b) Orientations of fold axes and poles to axial surfaces of folds in siliceous claystone; lower hemisphere, equal-area projection.

2.4 Raman Spectroscopic analysis

2.4.1 Samples and methods

To examine whether the evidence for increased heating can be detected from fault rocks, the RSCM was used. The samples for the Raman spectroscopic analysis were taken from the discrete slip surface and the scaly foliated carbonaceous claystone near the slip surface. We used a laser Raman microscope equipped with a 514.5 nm Ar^{+} laser and 50× objective lens. The exposure time was 10 s under 0.7 mW of the laser power to avoid thermal damage to the carbonaceous materials. We prepared 1.5 cm × 1.5 cm × 0.5 cm chips from the discrete slip surface and measured the RSCM on the surface. Thin sections were made to obtain the RSCM from the scaly foliated carbonaceous claystone, and the carbonaceous materials completely embedded within the rocks were analyzed. The obtained Raman spectra were corrected to remove the background effect by subtracting the linear baseline in the range of 1000–1800 cm^{-1}. Using the PeakFit v4.12 from SYSTAT Software Inc., the spectra were decomposed into D1-, D2-, D3- and D4-bands with a pseudo-Voigt function (Gaussian-Lorentzian sum), whose peak positions were near 1350 cm^{-1}, 1590 cm^{-1}, 1510 cm^{-1}, and 1245 cm^{-1}, respectively (Kouketsu et al., 2014).

2.4.2 Results

We analyzed the RSCM at 80 points from the discrete slip surface and the scaly foliated carbonaceous claystone. The representative Raman spectra and decomposed peaks are shown in Figures 2-7a and 2-7b, respectively. Compared to the RSCM in the scaly foliated carbonaceous claystone, the carbonaceous materials on the discrete slip surface show slightly increased D1-band intensity. The average I_{D1}/I_{D2} value of the scaly foliated carbonaceous claystone was 0.55 with a standard deviation (SD) of 0.03, whereas the discrete slip surface showed a higher average I_{D1}/I_{D2} value of 0.59 (SD 0.05) (Figure 2-7c). This indicates a slightly increased carbonization in the discrete slip surface relative to the surrounding scaly foliated carbonaceous claystone.

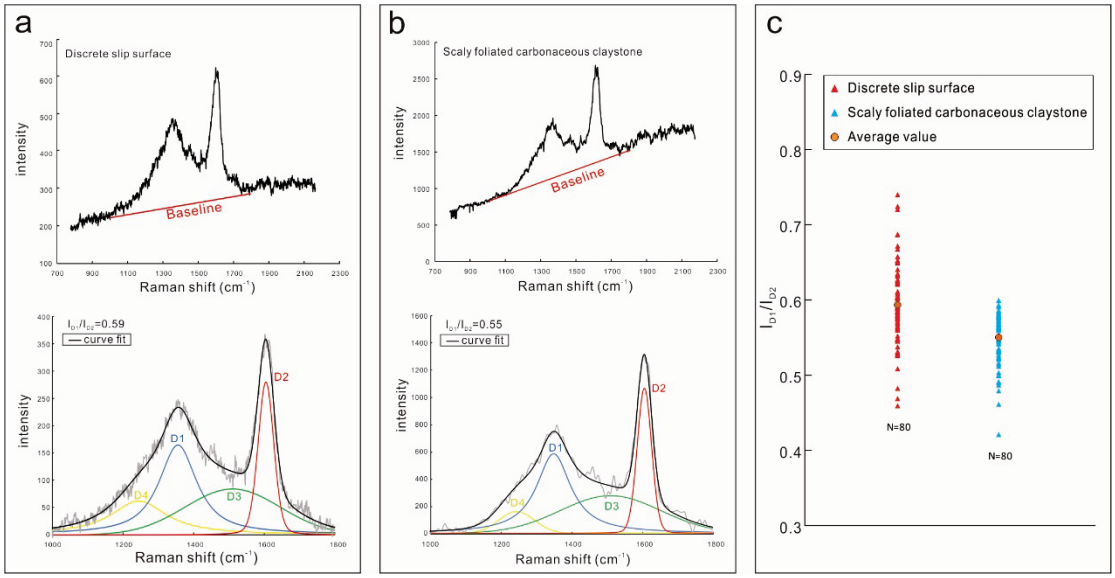

Figure 2-7 Representative Raman spectra and decomposed peaks of carbonaceous materials for (a) discrete slip surface and (b) scaly foliated carbonaceous claystone. (c) I_{D1}/I_{D2} values of the scaly carbonaceous claystone and discrete slip surface.

2.5 Discussion

Deformation in the fault zone partitioned into shearing along scaly carbonaceous claystone and localized slip along the discrete surface.

The kinematics of folds in siliceous claystone indicate top-to-the-SSE shear. This is consistent with the inferred shear direction during subduction of pelagic sediments (Kimura and Hori, 1993; Kimura, 1997, 1999). Assuming that the deformation-diagenetic model proposed by Snyder et al., (1983) and Brueckner et al., (1987) applied for the folding in chert, Kimura and Hori (1993) interpreted that the folds in chert were developed under opal-CT diagenetic conditions at temperatures below 165 °C, i.e., the maximum temperature of the transformation of opal-CT to quartz (Mizutani, 1977). Assuming that microcrystalline quartz in siliceous claystone underwent the same silica diagenesis as chert, the geometry and kinematics of the folds are interpreted to represent the subduction-related deformation under opal-CT diagenetic conditions.

The intense development of scaly fabric in the black carbonaceous claystone with respect to the upper mudstone in sheet 2 and foliated cataclasite represents the concentration of shear deformation. In the chert-clastic complex in the Inuyama area, the décollement is considered to be located in the siliceous claystone (Kimura and Hori, 1993). Our observation suggests that the shear strain was localized along the black carbonaceous claystone after the transformation of opal-CT to quartz. This could be due to the increased shear strength of siliceous claystone after the completion of silica diagenesis and the relative weakness of more clay-rich carbonaceous claystone because

the frictional strength decreases with increasing clay content (Tembe et al., 2010).

The scaly foliated carbonaceous claystone is distributed at four horizons in the fault zone. If the carbonaceous claystone represents the claystone accumulated during the climax of the deep-sea anoxic event that occurred across the Permian-Triassic boundary (Isozaki, 1997), four occurrences of carbonaceous claystone may represent the repetition of the same claystone by thrust faulting. Alternatively, four carbonaceous claystone layers were intercalated in siliceous claystone (Suzuki et al., 1998) and subsequently underwent intense shearing.

The kinematics of the fault zone indicate both reverse slip and left-lateral slip. This may represent heterogeneous slip directions during thrusting. Alternatively, the coexistence of reverse slip and left-lateral slip could be due to the slip partitioning associated with the left-lateral oblique subduction.

The increased carbonization in the discrete slip surface relative to the surrounding scaly foliated carbonaceous claystone represents the increased heating associated with the localized slip along the discrete slip surface (Figure 2-7c). The I_{D1}/I_{D2} values in the discrete slip surfaces (average 0.59) are lower than those in the pseudotachylyte, which recorded a melting temperature higher than 1100 °C (Ito et al., 2017; Ujiie et al., 2007; 2021). This suggests a smaller temperature rise in the discrete slip surface, consistent with the absence of frictional melting related deformation. The increased temperature recorded on the discrete slip surface appears to indicate that part of the left-lateral slip is accommodated by the seismic slip in deeper portions of the

subduction zone.

2.6 Conclusion

The plate-boundary faulting in deeper portions of the cold subduction zone was characterized by the localization of shear along carbonaceous claystone. Deformation in carbonaceous claystone is accommodated by the distributed shear along scaly foliations and localized slip along discrete surfaces. The kinematics of the fault zone indicate both reverse slip and left-lateral slip, possibly representing left-lateral oblique subduction or heterogeneous shear. The RSCM demonstrated a slight increase in carbonization in the discrete slip surface relative to the surrounding scaly carbonaceous claystone, suggesting that the localized slip along the discrete slip surface is accompanied by a coseismic temperature increase.

References

Brueckner, H. K., Snyder, W. S. and Boudreau, M. (1987). Diagenetic controls on the structural evolution of siliceous sediments in the Golconda allochthon, Nevada, U.S.A. Journal of Structural Geology, 9(4), 403–417.

Chester, F. M., Rowe, C., Ujiie, K., Kirkpatrick, J., Regalla, C., Remitti, F., Moore, J. C., Toy, V., Wolfson-Schwehr, M., Bose, S., Kameda, J., Mori, J. J., Brodsky, E. E., Eguchi, N., Toczko, S., and Expedition 343 & 343T Scientists. (2013). Structure and Composition of the Plate-Boundary Slip Zone for the 2011 Tohoku-Oki Earthquake. Science, 342(6163), 1208–1211.

Cowan, D. S. (1999). Do faults preserve a record of seismic slip? A field geologist's opinion. Journal of Structural Geology, 21(8–9), 995–1001.

Furuichi, H., Ujiie, K., Kouketsu, Y., Saito, T., Tsutsumi, A. and Wallis, S. (2015). Vitrinite reflectance and Raman spectra of carbonaceous material as indicators of frictional heating on faults: Constraints from friction experiments. Earth and Planetary Science Letters, 424, 191–200.

Ishikawa, T. and Ujiie, K. (2019). Geochemical analysis unveils frictional melting processes in a subduction zone fault. Geology, 47(4), 343–346.

Isozaki, Y. (1997). Permo-Triassic boundary superanoxia and stratified superocean: Records from lost deep sea. Science, 276(5310), 235–238.

Ito, K., Ujiie, K. and Kagi, H. (2017). Detection of increased heating and estimation of

coseismic shear stress from Raman spectra of carbonaceous material in pseudotachylytes. Geophysical Research Letters, 44(4), 1749–1757.

Kameda, J., Hina, S., Kobayashi, K., Yamaguchi, A., Hamada, Y., Yamamoto, Y., Hamahashi, M. and Kimura, G. (2012). Silica diagenesis and its effect on interplate seismicity in cold subduction zones. Earth and Planetary Science Letters, 317–318, 136–144.

Kimura, K. and Hori, R. (1993). Offscraping accretion of Jurassic chert-clastic complexes in the Mino-Tamba belt, central Japan. Journal of Structural Geology, 15(2), 145–161.

Kimura, K. (1997). Offscraping underplating and out-of-sequence thrusting process of an accretionary prism: On-land example from the Mino-Tanba Belt, central Japan. Bulletin of the Geological Survey of Japan, 48, 313-338.

Kimura, K. (1999). The slip direction of thrust faults-A case study from a chert-clastic sequence in the Mino-Tamba Belt, central Japan. Journal of Geological Society of Japan 105, 105, 208-226.

Kouketsu, Y., Mizukami, T., Mori, H., Endo, S., Aoya, M., Hara, H., Nakamura, D. and Wallis, S. (2014). A new approach to develop the Raman carbonaceous material geothermometer for low-grade metamorphism using peak width. Island Arc, 23(1), 33–50.

Kuo, L. W., Di Felice, F., Spagnuolo, E., Di Toro, G., Song, S. R., Aretusini, S., Li, H., Suppe, J., Si, J. and Wen, C. Y. (2017). Fault gouge graphitization as evidence of past

seismic slip. Geology, 45(11), 979–982.

Kuo, L. W., Li, H., Smith, S. A. F., Di Toro, G., Suppe, J., Song, S. R., Nielsen, S., Sheu, H. S. and Si, J. (2014). Gouge graphitization and dynamic fault weakening during the 2008 Mw 7.9 Wenchuan earthquake. Geology, 42(1), 47–50.

Labaume, P., Maltman, A. J., Bolton, A., Teissier, D., Ogawa, Y. and Takizawa, S. (1997). Scaly fabrics in sheared clays from the décollement zone of the Barbados accretionary prism. Proceedings of the Ocean Drilling Program, 156 Scientific Results, 156.

Matsuda, T. and Isozaki, Y. (1991). Well-documented travel history of Mesozoic pelagic chert in Japan: From remote ocean to subduction zone. Tectonics, 10(2), 475–499.

Mizutani, S. (1977). Progressive ordering of cristobalitic silica in the early stage of diagenesis. Contributions to Mineralogy and Petrology, 61(2), 129–140.

Moore, J. C. and Klaus, A. (2000). Synthesis of results: logging while drilling, northern Barbados accretionary prism. Proceedings of the Ocean Drilling Program, Scientific Results, 171(December 1999), 1–25.

Moore, J. C., Klaus, A., Bangs, N. L., Bekins, B., Bücker, C. J., Brückmann, W., Erickson, S. N., Hansen, O., Horton, T., Ireland, P., Major, C. O., Moore, G. F., Peacock, S., Saito, S., Screaton, E. J., Shimeld, J. W., Stauffer, P. H., Taymaz, T., Teas, P. A. and Tokunaga, T. (1998). Consolidation patterns during initiation and evolution of a plate-boundary decollement zone: northern Barbados accretionary prism. Geology, 26(9), 811–814.

Oohashi, K., Hirose, T. and Shimamoto, T. (2011). Shear-induced graphitization of carbonaceous materials during seismic fault motion: Experiments and possible implications for fault mechanics. Journal of Structural Geology, 33(6), 1122–1134.

Rowe, C. D. and Griffith, W. A. (2015). Do faults preserve a record of seismic slip: A second opinion. Journal of Structural Geology, 78, 1–26.

Snyder, W. S., Brueckner, H. K. and Schweickert, R. A. (1983). Deformational styles in the Monterey Formation and other siliceous sedimentary rocks. In I. CM & R. Garrison (Eds.), Petroleum Generation and Occurrence in the Miocene Monterey Formation (pp. 151–170).

Suzuki, N., Ishida, K., Shinomiya, Y. and Ishiga, H. (1998). High productivity in the earliest Triassic ocean: Black shales, Southwest Japan. Palaeogeography, Palaeoclimatology, Palaeoecology, 141(1–2), 53–65.

Takahashi, S., Oba, M., Kaiho, K., Yamakita, S., & Sakata, S. (2009). Panthalassic oceanic anoxia at the end of the Early Triassic: A cause of delay in the recovery of life after the end-Permian mass extinction. Palaeogeography, Palaeoclimatology, Palaeoecology, 274(3-4), 185-195.

Takahashi, S., Yamasaki, S., Ogawa, K., Kaiho, K. and Tsuchiya, N. (2015). Redox conditions in the end-Early Triassic Panthalassa. Palaeogeography, Palaeoclimatology, Palaeoecology, 432, 15–28.

Tembe, S., Lockner, D. A. and Wong, T. F. (2010). Effect of clay content and mineralogy on frictional sliding behavior of simulated gouges: Binary and ternary mixtures of

quartz, illite, and montmorillonite. Journal of Geophysical Research: Solid Earth, 115(3), 1–22.

Ujiie, K., and Kimura, G. (2014). Earthquake faulting in subduction zones: insights from fault rocks in accretionary prisms. Progress in Earth and Planetary Science, 1(1), 1–30.

Ujiie, K., Ito, K., Nagate, A. and Tabata, H. (2021). Frictional melting and thermal fracturing recorded in pelagic sedimentary rocks of the Jurassic accretionary complex, central Japan. Earth and Planetary Science Letters, 116638.

Ujiie, K., Tanaka, H., Saito, T., Tsutsumi, A., Mori, J. J., Kameda, J., Brodsky, E. E., Chester, F. M., Eguchi, N., Toczko, S. and Expedition 343 & 343T Scientists. (2013). Low coseismic shear stress on the Tohoku-Oki megathrust determined from laboratory experiments. Science, 342(6163), 1211–1214.

Ujiie, K., Yamaguchi, H., Sakaguchi, A. and Toh, S. (2007). Pseudotachylytes in an ancient accretionary complex and implications for melt lubrication during subduction zone earthquakes. Journal of Structural Geology, 29(4), 599–613.

Yamaguchi, A., Hina, S., Hamada, Y., Kameda, J., Hamahashi, M., Kuwatani, T., Shimizu, M., and Kimura, G. (2016). Source and sink of fluid in pelagic siliceous sediments along a cold subduction plate boundary. Tectonophysics, 686, 146–157.

Yamakita, S., Kaiho, K., Fujibayashi, M., Takahashi, S. and Kojima, S. (2010) Smithian/Spathian boundary in the Lower Triassic ocean-floor sequence of the Momotaro-Jinja section, Inuyama, central Japan. In: Abstracts of the 2010 annual

meeting of the palaeontological society of Japan, Tsukuba, 10-13 June 2010.

Yamakita, S., Takahashi, S. and Kojima, S. (2016) Conodont-based age-determination of siliceous claystone in the lower part of the Momotaro-jinja section, Inuyama, central Japan. In: Abstracts of the 2016 annual meeting of the palaeontological society of Japan, Kyoto University, Kyoto, 29-31 January 2016.

Yao, A. (1980). Triassic and Jurassic radiolarians from the Inuyama area, central Japan. Journal of Geosciences, Osaka City University, 23, 135–154.

Acknowledgments

At the outset, I would like to express my deepest gratitude to my dedicated supervisor, Associate Professor Kohtaro Ujiie, for his constant encourageme nt and guidance. He has walked me through all stages of accomplishing this thesis. I gratefully thank him for generous support and assistance and caring throughout my years at University of Tsukuba. I am very thankful to Professor Katsuo Sashida for providing me radiolarian biostratigraphy of the Lake Hamana area. I also thank Professor Hiroyuki Kagi for his caring support and advice during the Raman Spectroscopic analysis at the University of Tokyo.

I would like to express my heartfelt gratitude to Keisuke Ito, Ginta Motohashi, Ayaka Nagate, Chizuru Ozawa, who give me a lot of help in the field and laboratory analysis. I appreciate Frank Madison for the valuable comments and suggestions on the early version of the manuscript. I thank all members of Ujiie's laboratory for their help and useful discussion.

And I also express thanks to my dearest friends, Weiwei Chao, Fei Xue, Xinkai Hu, Qian Liu, and Yaping Hu, for their support during my study in Tsukuba.

Finally, I would like to extend my indebtedness to my family, especially my parents, for their continued support and generous care throughout my study.